MODELING OF ACOUSTIC NONLINEARITY CHANGE IN CONCRETE DUE TO MICROCRACKS PARTIALLY FILLED WITH ALCALI SILICA REACTION (ASR) GEL

A Master's Thesis
Presented to
The Academic Faculty

By

Denis Smajic

In Partial Fulfillment
of the Requirements for the Degree
Master of Science in Engineering Science and Mechanics in the
School of Civil and Environmental Engineering

Georgia Institute of Technology

December 2020

MODELING OF ACOUSTIC NONLINEARITY CHANGE IN CONCRETE DUE TO MICROCRACKS PARTIALLY FILLED WITH ALCALI SILICA REACTION (ASR) GEL

Approved by:

Professor Laurence J. Jacobs,
Advisor
School of Civil and Environmental Engineering
Georgia Institute of Technology

Dr. Jin-Yeon Kim
School of Civil and Environmental Engineering
Georgia Institute of Technology

Dr. Christine Valle
School of Mechanical Engineering
Georgia Institute of Technology

Date Approved: August 11, 2020

ACKNOWLEDGEMENTS

First of all, I would like to express my gratitude and appreciation to Professor Laurence J. Jacobs whose guidance, support and encouragement have been invaluable throughout my entire stay in Atlanta. He not only supported me with his inspiring experience and professional knowledge but also helped me handle all personal and organizational matters. I am grateful for his friendly attitude and the informal chats at the end of our meetings.
Secondly, I would like to say a special thank you to my supervisor Dr. Jin-Yeon Kim. His guidance and overall insight enabled me to gather comprehensive understanding of the field and thus allowed me to tackle challenging problems. He was very involved in my topic and showed an exceptional ability of critical thinking during our frequent meetings.

Furthermore, I would like to thank Professor Michael Hanss, Dominik Hose and Professor Peter Eberhard from the Institute of Engineering and Computational Mechanics in Stuttgart, Germany for selecting me as an appropriate candidate for this exchange program. Their guidance and support have been essential in order to fulfill all requirements concerning my studies at the Georgia Institute of Technology.

Last but not least, I want to thank my family for providing financial support to me and especially for the enjoyable times we had during our long videochats on weekends which almost made me feel like I was not missing anything back in Germany.

TABLE OF CONTENTS

LIST OF TABLES

LIST OF FIGURES

LIST OF SYMBOLS

Symbol	Description
∂	partial derivative operator
u_i	displacement vector
V	volume
$\boldsymbol{O}$	origin of cartesian coordinate system
F_{ij}	deformation gradient tensor
$\boldsymbol{X}, \boldsymbol{x}$	Lagrangian and Eulerian position vector
σ_{ij}	Cauchy stress tensor
$\boldsymbol{P}$	first Piola-Kirchhoff tensor
$\boldsymbol{E}$	Lagrangian strain tensor
$\boldsymbol{P}$	first Piola-Kirchhoff tensor
χ	mapping function
$B_0,\ B_t$	reference configuration, current configuration
W	strain energy density function
C_{ijkl}	fourth order stiffness tensor
C_{ijklmn}	sixth order stiffness tensor
$A,\ B,\ C$	third order elastic moduli by Landau & Schlitz
$l,\ m,\ n$	third order elastic moduli by Murnaghan
E	Young's Modulus
λ	first Lamé parameter
μ	second Lamé parameter
α_{cr}	linear coefficient of elasticity of a crack
β_{cr}	quadr. nonlinear coefficient of elasticity of a crack

table continues

continue table

Symbol	Description
F_i	force vector
x, y, z	cartesian coordinates
r	radial coordinate in cylindrical coordinate system
h	separation between two bodies
δ	displacement / Approach of two bodies
a	radius of a spherical body
p	pressure
p_0	pressure at $\boldsymbol{O}$
ρ_{L}	density of a liquid
s, ϕ	polar coordinates
a_{rel}	relative radius
F_{L}	lubrication force
μ_{L}	dynamic viscosity of a liquid
v	velocity
Δ, ∇^2	Laplacian operator
$\boldsymbol{\nabla}\cdot$	divergence operator
$\boldsymbol{\nabla}$	gradient operator
r_{u}, r_{c}	radial coordinates for lower/upper limit of liquid content
$u(x)$	substitution variable
$\bar{u}$	integration variable for integration by substition
R, A_{cr}	crack radius, crack area
R_{max}, σ_{R}	Max. crack radius, standard deviation of crack size distribution
S_{L}, S_{N}	lin. and nonlinear coefficients of compliance tensor

SUMMARY

Alkali silica reaction (ASR) is a complex, multi-scale chemomechanical process which can lead to the expansion and damage of concrete structures by forming microcracks, gradually reducing the structure's mechanical properties such as strength and stiffness.

This work investigates the effect of the ASR induced gel present within a microcrack on the material's nonlinear elastic constants. Therefore, significant changes such as the existence of lubrication need to be considered in addition to the contact force when deriving the stress state. The lubrication force depends on the viscosity and transport properties of the ASR gel and each of these needs to be modeled respectively. The characteristics of this force lead to the fact that nonlinearity due to microinhomogeneities is altered over time compared to the pure elastic contact force which is repulsive and tries to open the microcrack. Firstly, the contact force is approximated by a Hertzian contact between asperities, characterized by spherical tops located at different heights whereas the introduced lubrication force is derived in terms of the distance between irregularities and the gel volume present within a microcrack. As a second step, appropriate asperity distribution functions are used to derive the internal stress state within the crack which is then superimposed with the far field stress and the additional acoustic stress in order to express the nonlinear stress-strain relationship including the overall elastic constants of the solid. The higher order elastic constants are much more sensitive to microcracks than the Young's Modulus and Poisson's ratio which are altered only slightly due to the presence of microcracks. Nonlinear ultrasonic measurement techniques are capable of measuring second order waves which typically occur in nonlinear materials and relating these to the acoustic nonlinearity parameter β. The direct dependence of β on the quadratic and cubic nonlinearity parameters allows the derivation of a nonlinearity parameter relationship to the ASR gel volume present in a microcrack.

CHAPTER 1
INTRODUCTION

Concrete structures such as bridges, dry cask storage in power plants and buildings deteriorate with time due to material aging, chemical processes, thermal conditions, corrosion of embedded metals and cyclic mechanical loading. In order to improve the efficiency of servicing and maintenance, understanding these processes is essential towards predicting a structure's behavior accurately and determining the right intervals and types of maintenance.

Extensive experimental data have shown that strength parameters of a structure strongly depend on the stage of fatigue damage since the presence of discontinuities such as microcracks, voids and dislocations affect the magnitude of total load that a structure is able to bear reliably. Therefore, the demand for both nondestructive measurement techniques and computational models which are capable of relating measurements to certain damage stages has been increasing continuously.

One of the most important processes causing concrete deterioration is the alkali-silica reaction (ASR), often referred to as "concrete cancer" due to its difficulty to control and its severe consequences. The American Society for Testing and Materials (ASTM) has developed several test methods for screening of aggregates and their sensitivity to ASR, especially since widely known structures such as the "Adelaide Festival Centre" (Australia) or the "Maentwrog Dam" (Wales) have been demolished as a result of ASR.

1.1 Motivation and Objective

ASR is a complex, multi-scale chemomechanical process which can lead to the expansion and damage of concrete structures by forming microcracks and gradually reducing the structure's mechanical properties such as strength and stiffness. A representative volume

element (RVE) of concrete can be decomposed into silica-rich aggregates which are surrounded by a highly alkaline cement paste. The reaction of silica with the alkali ions causes the formation of an ASR gel layer at the common boundaries of the phases, the so called Interfacial transition zone (ITZ) as shown in figure 1.1. The pressure at the ITZ increases over time as water absorption leads to a swelling of the gel which results in the formation of microcracks once a critical pressure is exceeded. Since ASR can lead to critical structural problems in concrete, there is huge demand for accurate models that are able to interpret nondestructive measurements and predict the reduction of strength parameters.

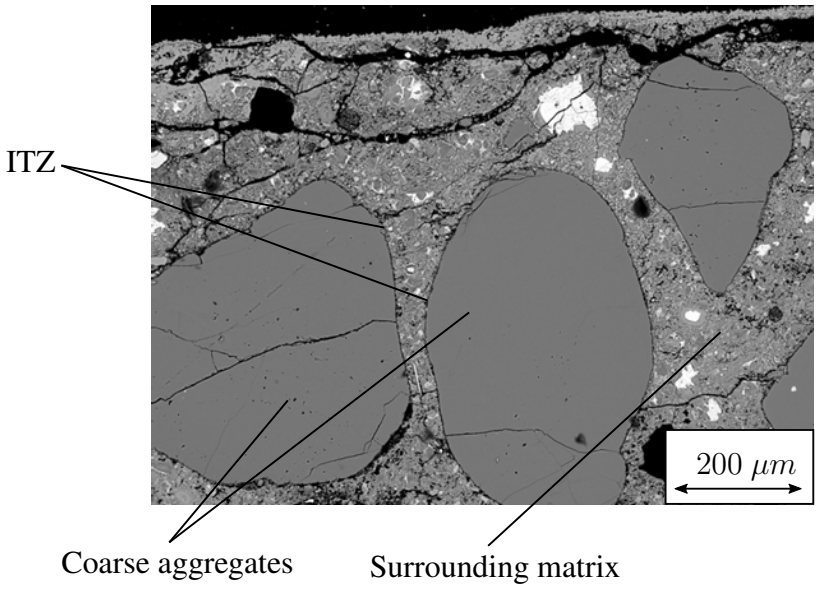

Figure 1.1: Microstructure of concrete

Inhomogeneities within a material such as dislocations, voids or microcracks generally behave in a nonlinear way with a magnitude that is closely related to the degree of fatigue damage of a structure. Widely performed experiments have shown that nonlinearities can be measured with ultrasonic waves, more precisely with nonlinear waves which are much more sensitive to crack sizes of the order of their wavelengths and smaller. In this case, a transducer is used to generate a bulk or a surface wave that propagates through the sample. A commonly used technique is the second harmonic generation where the ini-

tially generated wave, also called incident wave, interacts with the material's nonlinearities and generates a second harmonic wave of frequency which is double the frequency of the incident wave. The ratio of the incident to the second harmonic wave's amplitudes is proportional to the material nonlinearity such that a measurement of the wave amplitudes can provide important information about the material's nonlinearity. The nonlinearity can then be used to obtain structural defect parameters through respective models.

Since the transmitting and receiving transducers have to be fixed on the sample's surface, the measured ratio of amplitudes, referred to as β in the following, yields an average value over the measured volume and thus constraints the ability to perform localized measurements. Moreover, the measured nonlinearity can have multiple sources, e.g. measurement system nonlinearities. For this reason, further methods such as non-collinear wave mixing techniques have been developed to improve the accuracy of ultrasonic measurements and to provide new opportunities, particularly the generation of multiple waves from different sources which has the advantage of wave mixing at prescribed locations.

One of the main sources of material nonlinearity is the presence of microcracks. Initially, crack surfaces are flat and can be either open or closed, depending on the direction and magnitude of the applied stress. In these cases, the material's stiffness is reduced when the crack is opened whereas the initial stiffness is recovered once the crack closes. This phenomenon can be modeled using a bilinear stiffness material employing a Heaviside function for the case where the crack surfaces are closed and the overall stiffness increases. However, crack surfaces are not perfectly compatible due to grain detachment caused by multiple mechanisms including corrosion, electrical breakdown or repeated rubbing and fretting during crack closure. Therefore, the bilinear model can be only used to investigate the differences between fully closed and open crack surfaces, e.g. when the case of a partial closure can be neglected.

As rough crack surfaces approach each other due to an acoustic wave traveling through a sample, the number of interacting asperities increases. Consequently, the resistance of

the crack against closure increases as well, providing a highly nonlinear stress-strain relationship. This is a well studied behavior, although only valid for dry crack surfaces under the assumption of a negligible fluid pressure within the crack opening. Unlike the case of dry cracks, experiments performed on mortar samples indicate a saturation and decrease of the nonlinearity parameter β over time [1] which can have multiple conceivable causes, crack saturation with ASR gel being one of them. It is important to note that ASR gel is significantly less compressible than air, hence increasing the resistance of a crack against closure even before oppositely located asperities experience mechanical contact. Under those circumstances, the stress-strain curve of a microcrack could become less nonlinear when ASR gel effects are considered.

This work investigates the nonlinear stress-strain relationship in a cracked solid, containing partially filled microcracks with rough surfaces. For the sake of modeling the solid's behavior accurately, several forces including contact and lubrication effects need to be taken into account. The objective of this thesis is to derive a comparison between the nonlinearity of dry and wet cracks that are partially filled with ASR gel to different extents. The model will be subject to several assumptions and parameters for which a parametric study will be conducted for the purpose of establishing a dependency of the overall results on each parameter. Lastly, multiple crack orientations to the acoustic stress direction will be analyzed.

1.2 Thesis outline

The remaining chapters of this thesis are organized as follows. Chapter 2 gives an introduction to the theory related to this thesis, starting with a description of related work in this field. Afterwards, the main concepts of nonlinear elasticity are presented, followed by a derivation of contact forces between spherical bodies. Furthermore, the lubrication theory of two approaching spheres immersed in a liquid is extended to the case of partially covered spheres. This is essential for this work as different gel amounts cover the asperities to

different extents. The theory is completed by a derivation of a far field stress resulting from a given crack opening which is an important part of the solid's equilibrium state. Lastly, the chapter is concluded by a formulation of the overall problem.

Chapter 3 presents the formal description of the crack model developed in this work. First, a cracked RVE is briefly explained for better understanding of crack initiation in concrete samples, followed by a discussion of the assumptions on which the presented model is based. Subsequently, the interaction of rough surfaces is modeled before the pressure due to liquid present within the crack is integrated to obtain an expression for the force. The last part of this chapter deals with the integration of the force expression over all asperities to obtain the total pressure within the crack.

Chapter 4 first presents the evaluation of the results' dependency on the main model parameters. Once appropriate ranges for each parameter are obtained, simulations are performed such that a relation between the nonlinearities of dry and wet cracks can be established and related to the gel volume. Further, crack size distribution functions are simulated and discussed in order to investigate this effect on a solid's nonlinearity. Eventually, a qualitative analyisis of a nonlinearity development over time is conducted.

A summary of the results is given in the beginning of Chapter 5. Afterwards, a defense of the selected approach is provided whereby an outlook on further assessment possibilities for material nonlinearity is given. Last, alternative validation methods which would support the performed work with the developed model are addressed.

CHAPTER 2
THEORETICAL BACKGROUND

In the following, the main theoretical aspects needed to gain a detailed understanding of the developed model are addressed. Firstly, a brief summary of related work in this field is given for better classification of this work's contributions. Secondly, an explicit description of the main theoretical concepts is presented.

2.1 Related Work

A fundamental facet of this thesis is the elastic contact between two non-adhesive spheres (Hertzian contact) which is a well studied and extensively investigated topic, first introduced by Heinrich Hertz in 1881 and therefore named after him. Thenceforth, the contact theory has been adressed repeatedly in the past decades and can be found in several works such as Mindlin [2] and K.L. Johnson [3]. In general, approximating the contact of rough surfaces during an acoustic wave using the Hertzian contact theory is a widely adopted approach. Sevostianov and Kachanov [4] developed a simple micromechanical model for the contact of rough surfaces to show the incremental normal stiffness of the crack interface as well as the electrical conductivity accross it. For the transition from contact force to normal stress, from which the incremental stiffness can be derived, a consideration of a nominally flat surface covered with a large number of asperities is needed. Greenwood and Williamson [5] first developed a theory for the normal elastic contact between a rough surface and a flat by deriving an expression between the normal stress and crack closure displacement and formulated the problem using a probability density function for the asperity top height distribution. Nazarov and Sutin [6] applied this approach to a nonlinear stress-strain relationship in order to extract the quadratic and cubic nonlinearity parameters of fractured media. Although considered a key paper for the current work, this article

contains some assumptions which are partially resolved in this thesis. For example, [6] investigates only exponential distributions of the crack asperities in order to maintain all calculations in an analytical manner. Experimental data have shown that other asperity height distributions such as Gaussian distribution can occur in concrete cracks as well. Therefore, the work in hand incorporates a numerical analysis of several probability functions. Furthermore, the liquid pressure within dry cracks in [6] has been considered low enough to be neglected. The same authors have investigated the nonlinearity of cracks partially filled with ideal and viscous liquids within the frame of a narrow elliptic crack with smooth surfaces ([7]). In doing so, they focused on solving the state equations of the liquids in order to establish a comparison between ideal and viscous fluid which is out of the scope of this work. The present analysis extends the crack content in [6] to ASR gel and incorporates its lubrication effect into the nonlinear stress strain relationship.

The motion of two solid spheres immersed in an incompressible liquid has been studied through theoretical analysis (Brenner [8], Lambert et al. [9]) implying a non-slip boundary condition for the fluid layer attached to the solid's surfaces. However, this approach leads to an instability of the lubrication force, also referred to as hydrodynamic, resistance or viscous force, when the distance between the solids approaches zero. Vinogradova [10] has addressed the phenomenon of a liquid film drainage between hydrophobic surfaces and derived an expression for the lubrication force in dependence on the slip length (section 2.4). Another method to obtain an accurate expression for the hydrodynamic force during drainage is the modeling of the liquid as a bi-viscous fluid with a distance dependent viscosity ([11]). The present work extends the pressure integration in [10] to the case of partially covered solids in order to enable the consideration of different ASR gel volumes within the crack and the accompanying coverage of the solids to different extents.

2.2 Nonlinear Elasticity

This section describes the theory of continuum mechanics needed to gain an understanding of how stress, deformation and strain of a body are related.

For many engineering applications, approximating the strain as a linear function of the stress works well for elastic deformations. The basic theory of linear elastic continuum mechanics can be found in several books, for example [12] and [13]. However, applying this simplification to specimens containing structural defects at micro-scale would lead to significant errors due to their highly nonlinear behavior and therefore the stress function needs to contain higher order powers of the strain.

2.2.1 Deformation and Strain

A continuous body B can be defined as a subset of a three-dimensional space whose points have the coordinates $\boldsymbol{X}$ relative to a fixed origin $\boldsymbol{O}$ in its reference configuration B_0. At some time $t \neq 0$, a point with the initial coordinates $\boldsymbol{X}$ can be described in its current configuration B_t with the relation $\boldsymbol{x} = \chi(\boldsymbol{X}, t)$, where $\chi(\boldsymbol{X}, t)$ is a mapping function which assigns to each material point $\boldsymbol{X}$ in B_0 at time t a point $\boldsymbol{x}$ in B_t as shown in Figure 2.1. The mapping function is invertible and thus the relation

$$\boldsymbol{X} = \chi^{-1}(\boldsymbol{x}, t) \tag{2.1}$$

holds. The displacement of a point is given by

$$\boldsymbol{u}(\boldsymbol{X}, t) = \boldsymbol{x} - \boldsymbol{X} = \chi(\boldsymbol{X}, t) - \boldsymbol{X} \tag{2.2}$$

and the local deformation is described by the deformation gradient tensor

$$\boldsymbol{F} = \frac{\partial \boldsymbol{x}}{\partial \boldsymbol{X}} \quad \text{or} \quad F_{ij} = \frac{\partial x_i}{\partial X_j} \tag{2.3}$$

when indicial notation is used. The summation (Einstein) notation over repeated indices will be used in all indicial expressions, unless otherwise stated.

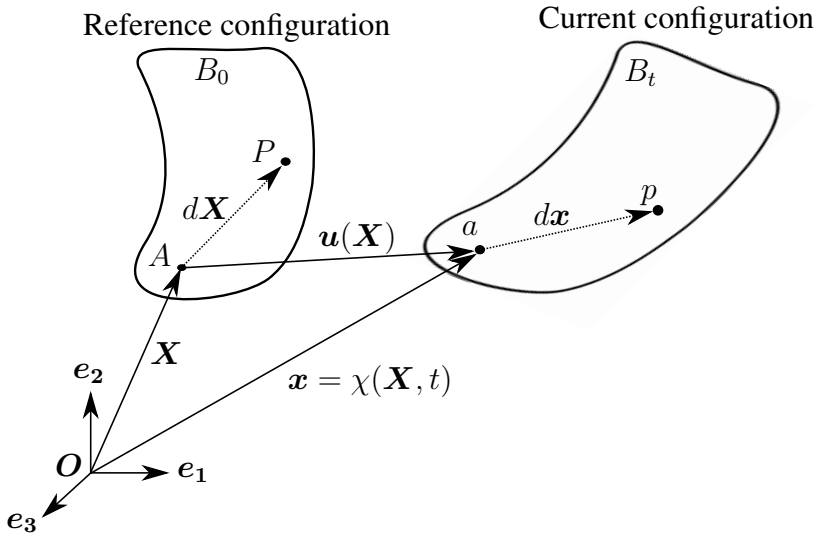

Figure 2.1: Reference and current configuration of a continuum

Further, the Lagrangian finite strain tensor is defined as

$$\boldsymbol{E} = \frac{1}{2}\left(\boldsymbol{F}^{\mathrm{T}}\boldsymbol{F} - \boldsymbol{I}\right) \quad \text{or} \quad E_{ij} = \frac{1}{2}\left(\frac{\partial u_i}{\partial X_j} + \frac{\partial u_j}{\partial X_i} + \frac{\partial u_k}{\partial X_i}\frac{\partial u_k}{\partial X_j}\right) \tag{2.4}$$

and can be reduced to

$$E_{ij} = \frac{1}{2}\left(\frac{\partial u_i}{\partial X_j} + \frac{\partial u_j}{\partial X_i}\right) = \frac{1}{2}\left(u_{i,j} + u_{j,i}\right) \tag{2.5}$$

for sufficiently small strains due to the negligible effect of the quadratic term ($|\frac{\partial u}{\partial X}| << 1$). The strain tensor is an appropriate measure for the elastic deformation and vanishes for a purely rigid motion.

2.2.2 Stress

The most widely used description for stress is the Cauchy stress tensor $\boldsymbol{\sigma}$ which decomposes an acting stress vector into three stress vector acting on mutually orthogonal surfaces.

This has the advantage that the multiplication of the stress tensor with the normal of any surface area of the deformed body (Eulerian coordinates) yields the traction vector accross the surface. More detailed description of the Cauchy stress tensor can be found in [14] and will be omitted in this work since all other quantities were introduced in terms of Lagrangian coordinates. Instead, a useful representation for the stress is introduced by

$$\boldsymbol{P} = \det\boldsymbol{F}\boldsymbol{\sigma}\boldsymbol{F}^{-\mathrm{T}} \tag{2.6}$$

where $\boldsymbol{P}$ is referred to as the first Piola-Kirchhoff stress tensor and transforms the stress to surface areas in Lagrangian coordinates.

Using the divergence theorem and the law for conservation of mass, an expression for the mechanical energy balance of the system can be derived. This expression contains the so called strain-energy density function W which represents a measure for the stored elastic energy in the system and thus depends on the principal strains λ_i. A detailed derivation of the constitutive relation for hyperelastic materials can be found in [15], leading to

$$\boldsymbol{P} = \boldsymbol{F}\frac{\partial W}{\partial \boldsymbol{E}} \quad \text{or} \quad P_{ij} = F_{ik}\frac{\partial W}{\partial E_{kj}} \tag{2.7}$$

The scalar strain-energy density function W can be approximated using a Taylor series expansion up to the third order term which yields

$$W \approx \frac{1}{2!}C_{ijkl}E_{ij}E_{kl} + \frac{1}{3!}C_{ijklmn}E_{ij}E_{kl}E_{mn} \tag{2.8}$$

where C_{ijkl} and C_{ijklmn} are constant components of a fourth order and a sixth order stiffness tensor, respectively. Due to the assumption that W is a scalar function and the symmetry of the strain tensor, $E_{ij} = E_{ji}$, certain symmetries of the tensors C_{ijkl} and C_{ijklmn} can be established. It is worth noting that the constant and linear term in the Taylor series expansion have been omitted since the energy density function is required to equal zero

and have a minimum for purely rigid motions.

Including the obtained expressions for W and E_{ij} and after carying out all partial derivatives, the constitutive relation becomes

$$P_{ij} = C_{ijkl}\frac{\partial u_k}{\partial X_l} + \frac{1}{2}M_{ijklmn}\frac{\partial u_k}{\partial X_l}\frac{\partial u_m}{\partial X_n} \tag{2.9}$$

with $M_{ijklmn} = C_{ijklmn} + C_{ijln}\delta_{km} + C_{jnkl}\delta_{im} + C_{jlmn}\delta_{ik}$.

2.2.3 1D stress-strain relationship for isotropic materials

In the case of isotropic symmetry, i.e. the stiffness components are identical in all directions, the simplifications

$$\begin{aligned} C_{ijkl} =& \lambda\delta_{ij}\delta_{kl} + \mu\left(\delta_{ij}\delta_{kl} + \delta_{il}\delta_{jk}\right) \\ C_{ijklmn} =& \, 2C\delta_{ij}\delta_{kl}\delta_{mn} + 2B(\delta_{ij}I_{klmn} + \delta_{kl}I_{mnij} + \delta_{mn}I_{ijkl}) + \\ & \frac{1}{2}A(\delta_{ik}I_{jlmn} + \delta_{il}I_{jkmn} + \delta_{jk}I_{ilmn} + \delta_{jl}I_{ikmn}) \end{aligned} \tag{2.10}$$

of the stiffness tensors can be obtained, where $I_{ijkl} = \frac{1}{2}(\delta_{ik}\delta_{jl} + \delta_{il}\delta_{jk})$. The parameters λ and μ are known as Lamé parameters and A, B and C are referred to as third-order elastic moduli, defined by Landau and Schlitz. Further similar expressions for the third-order elastic moduli have been defined by Murnaghan [16] as l, m and n.

In the case of an one-dimensional acoustic wave traveling through an elastic half space, the normal component of the first Piola-Kirchhoff stress tensor (in absence of transverse strain) can be written as

$$\begin{aligned} P_{11} =& C_{1111}\frac{\partial u_1}{\partial X_1} + \frac{1}{2}\left(M_{111111}\right)\frac{\partial u_1}{\partial X_1}\frac{\partial u_1}{\partial X_1} \\ =& C_{1111}\epsilon_{11} + \frac{1}{2}\left(C_{111111} + 3C_{1111}\right)\epsilon_{11}^2 \\ =& \left(\lambda + 2\mu\right)\epsilon_{11} + \frac{1}{2}\left(2C + 6B + 2A + 3\left(\lambda + 2\mu\right)\right)\epsilon_{11}^2 \end{aligned} \tag{2.11}$$

Rewriting the equation in terms of Murnaghan constants using the relations

$$\begin{aligned} A &= n \\ B &= m - \frac{1}{2}n \\ C &= l - m + \frac{1}{2}n \end{aligned} \tag{2.12}$$

one obtains

$$\begin{aligned} P_{11} &= (\lambda + 2\mu)\,\epsilon_{11} + \frac{1}{2}\left(3\,(\lambda + 2\mu) + 2\,(l + 2m)\right)\epsilon_{11}^2 \\ &= (\lambda + 2\mu)\left(\epsilon_{11} + \frac{1}{2}\underbrace{\left(3 + \frac{2\,(l + 2m)}{\lambda + 2\mu}\right)}_{\beta}\epsilon_{11}^2\right) \end{aligned} \tag{2.13}$$

from which the nonlinearity parameter β of a cracked medium can be extracted.

2.3 Contact Mechanics - Hertzian Approximation

Contact mechanics is the study of deformations and stresses within bodies which touch each other. Due to its wide applicability in engineering applications, the mechanics of a contact has been studied for different body geometries, yielding conditions such as pure elastic or elastoplastic cases and boundary conditions such as rigidity of one of the bodies. Some of its essential application fields include bearing design, transmission gearboxes, combustion engines but also the investigation of a microcrack's behavior during acoustic stresses.

The first commonly accepted analysis of contact stresses was introduced by Heinrich Hertz [17] who specified the displacement conditions within and outside the contact area during the approach of two elastic bodies, assuming that the contact area is small compared to the body dimensions and relative curvatures. Further assumptions of the Hertzian contact theory are listed in the following:

- the contact is non-adhesive and frictionless
- the surfaces are continuous, smooth and non-conforming
- the strains are small (elastic regime) such that the contact area radius is much smaller than the radius of each body
- each body acts as an elastic half-space

Using these conditions, the required displacement field can be derived, followed by specifying a satisfying pressure distribution. The following derivation complies with the notation in [3].

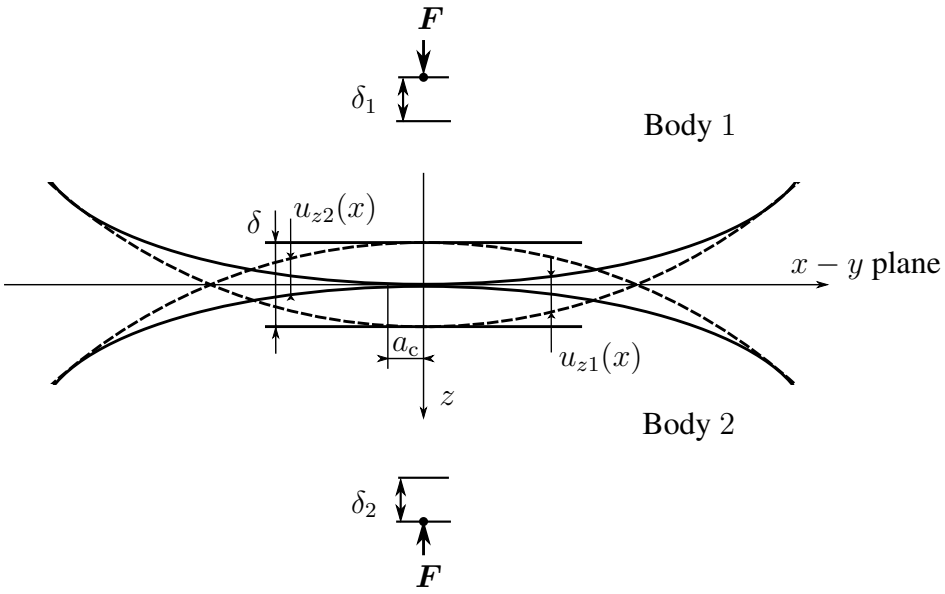

Figure 2.2: Hertzian elastic contact

Consider the case of two identical elastic spheres of radius a being brought into contact by a normal compressive load $\boldsymbol{F}$, applied at distant points of the spheres and acting along the coordinate axis z. The dashed line shows the undeformed configuration of the spheres whereas the solid lines represent the contacting surfaces. Immediately after the load is applied, the initial point of contact spreads to a circle of radius a_{c}. The separation between

the surfaces before loading can be described by

$$h\left(x,y\right)=\frac{1}{a}x^{2}+\frac{1}{a}y^{2} \tag{2.14}$$

Due to the pressure on the spheres, each surface is displaced by the same amount u_{z1} and u_{z2} for which the following statement can be made for all points x, y within the contact area

$$\begin{aligned} u_{z1}\left(x,y\right)+u_{z2}\left(x,y\right)+h\left(x,y\right)&=\delta=\delta_{1}+\delta_{2}\\ \rightarrow u_{z1}\left(x,y\right)+u_{z2}\left(x,y\right)&=\delta-\frac{1}{a}x^{2}-\frac{1}{a}y^{2} \quad \text{or}\\ u_{z1}\left(r\right)+u_{z2}\left(r\right)&=\delta-\frac{1}{a}r^{2} \end{aligned} \tag{2.15}$$

when a radial coordinate r is used instead of x, y. Outside the contact area, the surfaces do not touch such that

$$u_{z1}\left(r\right)+u_{z2}\left(r\right)>\delta-\frac{1}{a}r^{2} \tag{2.16}$$

In order to obtain the force-displacement relationship $F\left(\delta\right)$, a pressure distribution needs to be found such that the normal displacements within and outside the contact area satisfy eq. (2.15) and equation (2.16).

It can be shown that the pressure distribution proposed by Hertz

$$p\left(r\right)=p_{0}\left(1-\left(\frac{r}{a_{\mathrm{c}}}\right)^{2}\right)^{\frac{1}{2}} \tag{2.17}$$

gives rise to such a displacement. A detailed derivation can be found in [3]. The respective normal displacement is obtained from the theory of potential and gives

$$u_{z}\left(r\right)=\frac{1-\nu^{2}}{\pi E}\int_{0}^{2\pi}\int_{0}^{a_{\mathrm{c}}}p\left(s,\phi\right)dsd\phi \tag{2.18}$$

where s and ϕ are polar coordinates of the surface area over which the pressure is dis-

tributed. Carrying out the integration yields

$$u_z(r) = \frac{1-\nu^2}{E}\frac{\pi p_0}{4a_\mathrm{c}}\left(2a_\mathrm{c}^2 - r^2\right), \quad r \leq a \tag{2.19}$$

for the normal displacement within the area of contact. Substituting the displacements of both spheres into eq. (2.15) along with the relative curvature $(1/a_\mathrm{rel}) = (1/a_1 + 1/a_2)$ gets

$$\frac{\pi p_0 (1-\nu^2)}{2a_\mathrm{c}E}\left(2a_\mathrm{c}^2 - r^2\right) = \delta - \frac{1}{2a_\mathrm{rel}}r^2 \tag{2.20}$$

In order to obtain valid expressions for the approach δ and the contact area radius a_c, the dependence on the radial coordinate has to vanish, i.e.

$$\begin{aligned} \frac{\pi p_0 (1-\nu^2)}{2a_\mathrm{c}E} = \frac{1}{2a_\mathrm{rel}} \rightarrow a_\mathrm{c} &= \frac{\pi p_0 (1-\nu^2) a_\mathrm{rel}}{E} \\ \delta &= \frac{\pi p_0 (1-\nu^2) a_\mathrm{c}}{E} \end{aligned} \tag{2.21}$$

from where the load-pressure relationship can be established by integrating over the contact area

$$F = \int_0^{a_\mathrm{c}} p(r)\, 2\pi r dr = p_0 \frac{2}{3}\pi a_\mathrm{c}^2 \tag{2.22}$$

Substituting the expressions from equation (2.21) into equation (2.22) eventually defines the force-displacement relationship

$$F(\delta) = \frac{4}{3}\frac{E}{2(1-\nu^2)} a_\mathrm{rel}^{\frac{1}{2}}\, \delta^{\frac{3}{2}} \tag{2.23}$$

with $a_\mathrm{rel} = 2a$ for two spherical solids of radius a and $a_\mathrm{rel} = a$ for the case of a sphere approaching a flat elastic half-space. This equation will be used to model the contact force of rough surfaces with asperities approximated by spherical tops.

2.4 Lubrication theory - drainage of a liquid film between approaching spheres

The lubrication theory as a branch of fluid dynamics describes the kinematics and kinetics of a fluid motion between solids. It is well known that solids can slide more easily over one another when a thin liquid film is squeezed between them. This phenomenon has been used widely in the field of tribology in order to substitute the high friction which occurs between solids with the much lower friction of a solid-fluid interface. In the case of solids moving towards each other, a lubrication layer can exert resistance forces on the solids before a mechanical contact occurs and thus reduce highly local variations in the pressure distribution close to the area of contact.

Carrying this aspect over to the nonlinear contact of rough crack surfaces, it is suitable to expect a smoother course of the pressure occurring within a crack during a dynamic approach of its surfaces in the presence of an ASR gel layer. In order to investigate the exact effect of the ASR gel layer, an appropriate expression for the hydrodynamic force in terms of the distance between the solids is required. Moreover, the wall-slip needs to be taken into account respectively since the gel layer is drained perpendicularly to the direction of motion as the solids are squeezed.

The slip of a liquid at solid boundaries was not detected until the middle of the 18th century when Navier first proposed a theory that slip might occur at solid boundary [18], yet being inconsistent with the state of knowledge at that time. For this reason, the assumption of a zero boundary slip was widely accepted and is still used as it yields boundary conditions which are easily to handle as well as sufficient approximations for large enough separations between the solids. However, the lubrication force approximation [19, 20], solved under a no-slip boundary condition (BC)

$$F_{\mathrm{L}} = \frac{6\pi\mu_{\mathrm{L}} a^2 v}{\delta} \tag{2.24}$$

yields a force singularity when the solids are brought into contact (separation distance

$\delta \to 0$) which physically makes sense since the liquid is assumed to stick to the solid's surfaces. The remaining parameters in equation (2.24) - μ_{L}, a and v represent the dynamic viscosity of the fluid, the radius of the spherical solids and their approaching velocity, respectively. In order to account for the lateral sliding motion of the fluid on the contacting interface, the boundary conditions need to be adjusted by considering wall-slip.

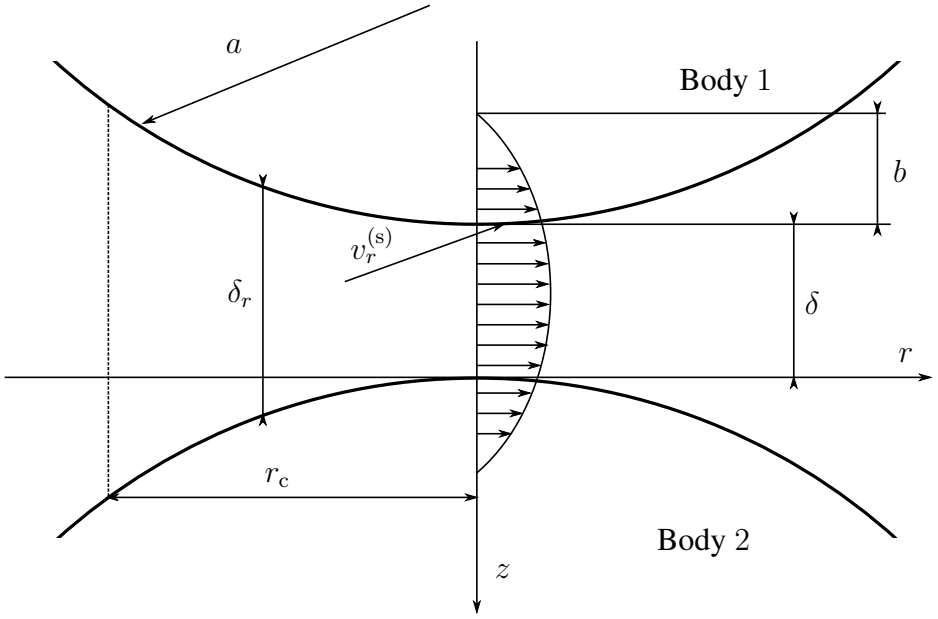

Figure 2.3: Schematic representation of one sphere approaching another

Figure 2.3 shows a schematic representation of two spheres immersed in a viscous liquid and separated by the distance δ. Due to rotational symmetries, a problem description in cylindrical coordinates is appropriate. For the purpose of a computationally efficient analytical solution, small errors due to the following assumptions are introduced:

- the solids act as rigid bodies and are approximated by paraboloids of revolution
- only normal collisions are considered and therefore no rotational motion occurs: $v_\phi = 0, \frac{\partial}{\partial \phi} = 0$; the motion is steady, $\frac{\partial}{\partial t} = 0$

- ASR gel behaves as a Newtonian liquid, i.e. shear stress linearly related to the shear strain rate by a constant parameter called dynamic viscosity μ_{L}
- the liquid is treated as a continuum at all times

2.4.1 Derivation of the pressure distribution function

The liquid motion is generally governed by the Navier-Stokes equations

$$\rho_{\mathrm{L}} \frac{\partial \boldsymbol{v}}{\partial t} + \rho_{\mathrm{L}} \boldsymbol{v} \cdot \boldsymbol{\nabla} \boldsymbol{v} + \boldsymbol{\nabla} p = \mu_{\mathrm{L}} \boldsymbol{\Delta} \boldsymbol{v} \tag{2.25}$$

and the continuity equation for incompressible fluids (based on the divergence theorem)

$$\boldsymbol{\nabla} \cdot \boldsymbol{v} = 0 \tag{2.26}$$

In vectorial notation, equations (2.25) and (2.26) yield the steady equations of fluid motion

$$\begin{aligned} r: \quad & \rho_{\mathrm{L}} \left(v_r \frac{\partial v_r}{\partial r} + v_z \frac{\partial v_r}{\partial z} \right) = -\frac{\partial p}{\partial r} + \mu_{\mathrm{L}} \left(\frac{1}{r} \frac{\partial}{\partial r} \left(r \frac{\partial v_r}{\partial r} \right) + \frac{\partial^2 v_r}{\partial z^2} - \frac{v_r}{r^2} \right) \\ z: \quad & \rho_{\mathrm{L}} \left(v_r \frac{\partial v_z}{\partial r} + v_z \frac{\partial v_z}{\partial z} \right) = -\frac{\partial p}{\partial z} + \mu_{\mathrm{L}} \left(\frac{1}{r} \frac{\partial}{\partial r} \left(r \frac{\partial v_z}{\partial r} \right) + \frac{\partial^2 v_z}{\partial z^2} \right) \end{aligned} \tag{2.27}$$

and the continuity equation

$$\frac{\partial v_z}{\partial z} + \frac{1}{r} \frac{\partial}{\partial r} \left(r v_r \right) = 0 \tag{2.28}$$

In order to introduce appropriate boundary conditions, the slip flow is characterized by a quantity referred to as the slip length b which measures the distance beyond the solid's surface, at which the radial velocity extrapolates to zero [21], as shown in figure 2.3. The slip length is defined as

$$v_r^{(\mathrm{s})} = b \left. \frac{\partial v_r}{\partial z} \right|_{z=\delta} \tag{2.29}$$

This relation is often used to link the slip to measurable macroscopic parameters such as wetting, shear rates or surface roughness. The boundary conditions then become

$$v_r = \begin{cases} b\frac{\partial v_r}{\partial z} & \text{at} \quad z = -\frac{1}{2}\frac{r^2}{a} \\ b\frac{\partial v_r}{\partial z} & \text{at} \quad z = \delta + \frac{1}{2}\frac{r^2}{a} \end{cases}$$

where the spherical bodies have been approximated as paraboloids of revolution. This assumption will be justified when the resulting lubrication force is derived. Furthermore, $v_z = 0$ at $z = -\frac{1}{2}\frac{r^2}{a}$ and $v_z = -v$ at $z = \delta + \frac{1}{2}\frac{r^2}{a}$ describe the boundary conditions for the vertical fluid motion, implying that Body 1 is approaching the fixed Body 2 with velocity v.

Equation (2.27) in the given form is complicated enough to prohibit an analytical solution to this problem. Reynold figured out that in "slow viscous motions", the pressure and viscous terms predominate [22]. In the case where the variation in two directions is significantly higher than in the third one (the variation of δ will be shown to be much smaller than characteristic dimensions in the r direction), the equations of motion reduce to

$$\begin{aligned} r: \quad & \frac{\partial p}{\partial r} = \mu_{\mathrm{L}} \left(\frac{\partial^2 v_r}{\partial z^2} \right) \\ z: \quad & \frac{\partial p}{\partial z} \approx 0 \end{aligned} \tag{2.30}$$

including the fact that the pressure only depends on the radial coordinate for steady-state conditions (shown in [22]). Integrating the radial component of equation (2.30) taking into account the boundary conditions for v_r involves a variable separation method and leads to

$$v_r = \frac{1}{2\mu_{\mathrm{L}}} \frac{\partial p}{\partial r} \left(z^2 - z\delta_r - b\delta_r \right) \tag{2.31}$$

where $\delta_r = \delta + \frac{r^2}{a}$ stands for the separation distance at r. Substituting equation (2.31) into

the continuity equation (2.28), the approaching velocity of Body 1 becomes

$$v = v_z^{(\mathrm{B}_1)} = \frac{1}{2\mu_\mathrm{L} r}\frac{\partial}{\partial r}\left[r\frac{\partial}{\partial r}\left(\frac{1}{3}\left(\delta + \frac{1}{2}\frac{r^2}{a}\right)^3 - \frac{\delta_r}{2}\left(\delta + \frac{1}{2}\frac{r^2}{a}\right)^2 - \left(\delta + \frac{1}{2}\frac{r^2}{a}\right) b\delta_r\right)\right] \tag{2.32}$$

which is in agreement with [10]. After integrating equation (2.32) two times with respect to r and plugging in $\frac{\partial p}{\partial r}$ at $r = 0$ (symmetry about the z axis) as well as $p = 0$ at $r = \infty$, the final expression for the pressure distribution

$$p(r) = \frac{\mu_\mathrm{L} a_\mathrm{eq} v}{\delta_r b} - \frac{\mu_\mathrm{L} a_\mathrm{eq} v}{6b^2}\ln\left(1 + \frac{6b}{\delta_r}\right) \tag{2.33}$$

is obtained, where $a_\mathrm{eq} = \frac{a}{2}$ for the case of two spheres and $a_\mathrm{eq} = a$ for the case of a sphere approaching a flat wall. In the following, the pressure function is integrated over the immersed surface area of the solids in order to obtain the lubrication force of the ASR gel.

2.4.2 Derivation of the lubrication force

Depending on the amount of ASR gel present within a crack, each pair of spherical asperities is covered by liquid to different extents. A relation between δ and the covered portion of a spherical top is established in chapter 3. This subsection is focused on deriving the lubrication force in terms of a radial coordinate r_c which characterizes the liquid layer width as shown in figure 2.3. A dashed line has been drawn only on the left side for the purpose of simplicity. In the case of a positive distance δ (spheres are not yet in contact), the lubrication force is given by

$$F_{\mathrm{L},\,\delta\geq 0} = \int_0^{r_\mathrm{c}} p\,(r)\,2\pi r dr = \frac{2\pi\mu_\mathrm{L} a_\mathrm{eq} v}{b}\int_0^{r_\mathrm{c}}\left(\frac{1}{\delta_r} - \frac{1}{6b}\ln\left(1 + \frac{6b}{\delta_r}\right)\right) r dr \tag{2.34}$$

Splitting equation (2.34) in three parts $F_{\mathrm{L},\,\delta\geq 0} = F_{\mathrm{L},1} + F_{\mathrm{L},2} + F_{\mathrm{L},3}$ yields

$$\begin{aligned} F_{\mathrm{L},1} &= \frac{2\pi\mu_{\mathrm{L}} a_{\mathrm{eq}} v}{b} \int_0^{r_{\mathrm{c}}} \frac{r}{\delta + \frac{r^2}{a}} dr \\ F_{\mathrm{L},2} &= -\frac{2\pi\mu_{\mathrm{L}} a_{\mathrm{eq}} v}{6b^2} \int_0^{r_{\mathrm{c}}} r \ln\left(\delta + \frac{r^2}{a} + 6b\right) dr \\ F_{\mathrm{L},3} &= \frac{2\pi\mu_{\mathrm{L}} a_{\mathrm{eq}} v}{6b^2} \int_0^{r_{\mathrm{c}}} r \ln\left(\delta + \frac{r^2}{a}\right) dr \end{aligned} \tag{2.35}$$

The necessity of approximating the spheres as paraboloids of revolution becomes apparent now. An analytical solution of the integrals in equation (2.35) is sought in order to maintain the exact dependence on δ and r_{c} wherefore the substitution $\bar{u} = u(r) = \delta + \frac{1}{2}\frac{r^2}{a_{\mathrm{eq}}}$ with $d\bar{u} = u'(r)dr = \frac{r}{a_{\mathrm{eq}}}dr \rightarrow dr = \frac{a_{\mathrm{eq}}}{r}d\bar{u}$ is introduced such that the integrals become

$$\begin{aligned} F_{\mathrm{L},1} &= \frac{2\pi\mu_{\mathrm{L}} a_{\mathrm{eq}}^2 v}{b} \int_{u(0)}^{u(r_{\mathrm{c}})} \frac{1}{\bar{u}} d\bar{u} \\ F_{\mathrm{L},2} &= -\frac{2\pi\mu_{\mathrm{L}} a_{\mathrm{eq}}^2 v}{6b^2} \int_{u(0)}^{u(r_{\mathrm{c}})} \ln\left(\bar{u} + 6b\right) d\bar{u} \\ F_{\mathrm{L},3} &= \frac{2\pi\mu_{\mathrm{L}} a_{\mathrm{eq}}^2 v}{6b^2} \int_{u(0)}^{u(r_{\mathrm{c}})} \ln\left(\bar{u}\right) d\bar{u} \end{aligned} \tag{2.36}$$

Carrying out the integration gives

$$\begin{aligned} F_{\mathrm{L},1} &= \frac{2\pi\mu_{\mathrm{L}} a_{\mathrm{eq}}^2 v}{b} \Big[\ln\left(\bar{u}\right)\Big]_{u(0)}^{u(r_{\mathrm{c}})} \\ F_{\mathrm{L},2} &= -\frac{2\pi\mu_{\mathrm{L}} a_{\mathrm{eq}}^2 v}{6b^2} \Big[(6b + \bar{u})\ln\left(6b + \bar{u}\right) - \bar{u}\Big]_{u(0)}^{u(r_{\mathrm{c}})} \\ F_{\mathrm{L},3} &= \frac{2\pi\mu_{\mathrm{L}} a_{\mathrm{eq}}^2 v}{6b^2} \Big[\bar{u}\left(\ln\left(\bar{u}\right) - 1\right)\Big]_{u(0)}^{u(r_{\mathrm{c}})} \end{aligned} \tag{2.37}$$

from where the final expression for the lubrication force components

$$
\begin{aligned}
F_{\mathrm{L},1} &= \frac{2\pi\mu_{\mathrm{L}} a_{\mathrm{eq}}^2 v}{b}\left[\ln\left(1+\frac{r_{\mathrm{c}}^2}{2a_{\mathrm{eq}}\delta}\right)\right] \\
F_{\mathrm{L},2} &= -\frac{2\pi\mu_{\mathrm{L}} a_{\mathrm{eq}}^2 v}{6b^2}\left[\left(6b+\delta+\frac{r_{\mathrm{c}}^2}{2a_{\mathrm{eq}}}\right)\ln\left(6b+\delta+\frac{r_{\mathrm{c}}^2}{2a_{\mathrm{eq}}}\right)-(6b+\delta)\ln(6b+\delta)-\frac{r_{\mathrm{c}}^2}{2a_{\mathrm{eq}}}\right] \\
F_{\mathrm{L},3} &= \frac{2\pi\mu_{\mathrm{L}} a_{\mathrm{eq}}^2 v}{6b^2}\left[\left(\delta+\frac{r_{\mathrm{c}}^2}{2a_{\mathrm{eq}}}\right)\left(\ln\left(\delta+\frac{r_{\mathrm{c}}^2}{2a_{\mathrm{eq}}}\right)-1\right)-\delta\left(\ln(\delta)-1\right)\right]
\end{aligned}
\tag{2.38}
$$

is obtained considering the substitutions $u(r_{\mathrm{c}}) = \delta + \frac{r_{\mathrm{c}}^2}{2a_{\mathrm{eq}}}$ and $u(0) = \delta$. It is worth noting that the dependence on r_{c} will be replaced by a value derived from the volume of ASR gel in chapter 3 once a suitable relation between these two parameters is established.

As soon as two oppositely located spherical asperities are brought into contact ($\delta < 0$), the given expression for the lubrication force is no longer applicable since the lower limit of integration has to be replaced by the value a_{c} which has already been introduced as the radius of contact area in figure 2.2. A detailed depiction of the correlation $a_{\mathrm{c}}(\delta, a)$ is deduced in chapter 3. Here, the lower limit of integration is denoted as r_{u}. Then, equation (2.34) adjusts to

$$
F_{\mathrm{L},\,\delta<0} = \int_{r_{\mathrm{u}}}^{r_{\mathrm{c}}} p\,(r)\,2\pi r dr = \frac{2\pi\mu_{\mathrm{L}} a_{\mathrm{eq}} v}{b}\int_{r_{\mathrm{u}}}^{r_{\mathrm{c}}}\left(\frac{1}{\delta_r}-\frac{1}{6b}\ln\left(1+\frac{6b}{\delta_r}\right)\right) r dr \tag{2.39}
$$

where splitting in three parts $F_{\mathrm{L},\,\delta<0} = F_{\mathrm{L},4} + F_{\mathrm{L},5} + F_{\mathrm{L},6}$ (similarly to the case $\delta \geq 0$) and taking the integrals gives

$$
\begin{aligned}
F_{\mathrm{L},4} &= \frac{2\pi\mu_{\mathrm{L}} a_{\mathrm{eq}}^2 v}{b}\left[\ln\left(\frac{2a_{\mathrm{eq}}\delta+r_{\mathrm{c}}^2}{2a_{\mathrm{eq}}\delta+r_{\mathrm{u}}^2}\right)\right] \\
F_{\mathrm{L},5} &= -\frac{2\pi\mu_{\mathrm{L}} a_{\mathrm{eq}}^2 v}{6b^2}\left[\left(6b+\delta+\frac{r_{\mathrm{c}}^2}{2a_{\mathrm{eq}}}\right)\ln\left(6b+\delta+\frac{r_{\mathrm{c}}^2}{2a_{\mathrm{eq}}}\right)\right. \\
&\quad \left.-\left(6b+\delta+\frac{r_{\mathrm{u}}^2}{2a_{\mathrm{eq}}}\right)\ln\left(6b+\delta+\frac{r_{\mathrm{u}}^2}{2a_{\mathrm{eq}}}\right)+\frac{r_{\mathrm{u}}^2-r_{\mathrm{c}}^2}{2a_{\mathrm{eq}}}\right]
\end{aligned}
$$

$$F_{\mathrm{L},6} = \frac{2\pi\mu_{\mathrm{L}} a_{\mathrm{eq}}^2 v}{6b^2}\left[\left(\delta + \frac{r_{\mathrm{c}}^2}{2a_{\mathrm{eq}}}\right)\left(\ln\left(\delta + \frac{r_{\mathrm{c}}^2}{2a_{\mathrm{eq}}}\right) - 1\right) - \left(\delta + \frac{r_{\mathrm{u}}^2}{2a_{\mathrm{eq}}}\right)\left(\ln\left(\delta + \frac{r_{\mathrm{u}}^2}{2a_{\mathrm{eq}}}\right) - 1\right)\right] \tag{2.40}$$

In order to achieve a complete expression for the lubrication force in terms of the relative approach δ, a smooth transition from $F_{\mathrm{L},\,\delta\geq 0}$ to $F_{\mathrm{L},\,\delta<0}$ has to take place at the point where the asperities touch. In its entirety, the force describes the drainage of a liquid film between two spherical bodies during a relative displacement caused by an acoustic wave traveling through a crack's interface.

2.5 Internal Stress in solid surrounding a penny-shaped crack

For the purpose of a detailed and formal problem formulation, one more technical aspect needs to be outlined. The preceding two sections were focused on stresses occurring due to compression of crack surfaces. However, since the crack is in equilibrium when no additional stresses act, the in-crack stress has to be compensated by some remote stress acting in the opposite direction. It seems reasonable that the surrounding solid provides a resistance against the opening of crack surfaces. Therefore, a relation between the crack opening displacement and the far field stress is sought in order to correlate the stress to the relative approach of crack surfaces. The problem is subject to the following assumptions:

- the compressive stress which occurs in the surrounding solid due to a crack opening displacement has the same magnitude as a tensile far field stress which opens the crack to the same extent
- the crack has the shape of a circular disk of radius R, also known as a penny-shaped crack
- the surrounding solid is isotropic and homogeneous
- the crack density is low enough such that interactions between cracks are negligible

The distribution of stress in the neighborhood of a penny-shaped crack in an elastic solid was first studied by Sneddon [23] and has been used in several works [24, 25]. The derivation involves solving a mixed boundary-value problem with the Collins' Method. Due to its complexity, the derivation is omitted here and the resulting stress-displacement relationship

$$u_z = \frac{2\,(1-\nu)\,p_0\sqrt{R^2-r^2}}{\pi\mu} = \frac{4\,(1-\nu^2)\,p_0\sqrt{R^2-r^2}}{\pi E} \tag{2.41}$$

is adopted, where E, μ, ν represent the solid's elastic parameters and p_0 denotes the remote stress. The respective crack volume is then given by

$$\begin{aligned} V &= \frac{4\,(1-\nu^2)\,p_0}{\pi E}\int_0^{2\pi}\int_0^{R}\int_{-\sqrt{R^2-r^2}}^{\sqrt{R^2-r^2}} r\,dz\,dr\,d\theta \\ V &= \frac{16\,(1-\nu^2)\,p_0 R^3}{3E} \end{aligned} \tag{2.42}$$

Therefore, the internal stress in the surrounding solid due to crack opening is related to the crack volume by

$$p_0 = \frac{3VE}{16\,(1-\nu^2)\,R^3} \tag{2.43}$$

This formula will be used in chapter 3 to link the remote stress p_0 to the crack opening δ in order to determine the equilibrium opening for different amounts of ASR gel.

2.6 Formal problem formulation

Nondestructive evaluation techniques (NDE) are capable of measuring the nonlinearity of concrete structures which has been shown to significantly depend on the amount and size of structural microdefects such as voids, dislocations and especially microcracks. As alkali-silica reaction takes place between silica-rich aggregates and the highly alkaline cement paste, the amount of a byproduct called ASR gel continuously increases until the pressure at the ITZ (figure 1.1) is sufficiently high to cause the formation of microcracks and the ASR gel to flow into those.

The nonlinearity parameter which has been measured throughout an entire ASR process has been found to first increase rapidly and then slowly decrease. The gel is expected to have the reducing effect on the nonlinearity of a microdefect. Therefore, a more complete model is required which is able to compute the total force acting within the crack for a prescribed amount of gel in terms of the distance between the crack surfaces. Consequently, the hydrodynamic force components of the gel (section 2.4) have to be combined with the mechanical contact force (section 2.3) between asperities in order to obtain a total force $F(\delta)$. To make the model sufficiently accurate, physical aspects such as volume conservation of the gel and flow properties need to be accounted for. Furthermore, appropriate functions which describe the crack surface textures adequately are sought in order to extend the interaction of a pair of asperities to an entire microcrack.

After all stresses acting on a crack are known, a question regarding the dependence of the stress state on the action of an acoustic wave arises. More precisely, the acoustic stress $\tilde{\sigma}$ caused by a crack surface distance variation $\tilde{\delta}$ has to be analyzed with regard to its nonlinearity.

A parametric study needs to be performed for the main parameters of the model. For parameters which can not be determined with certainty, acceptable ranges which are in compliance with experimental data have to be established. Finally, an analysis of the nonlinearity change over time under consideration of crack formation and crack filling with ASR gel is desired.

CHAPTER 3
MODELING OF ACOUSTIC NONLINEARITY CHANGE DUE TO ASR

The aim of this chapter is to develop a sufficiently sophisticated model, from which the nonlinearity of a cracked medium containing ASR gel can be obtained. To make the modeling approach more comprehensible, it is useful to start with a description of the crack initiation process in concrete samples.

3.1 Damaged RVE with microcrack initiation

As mentioned in the introduction, a representative volume element (RVE) of concrete can be understood as a composition of construction aggregates of different sizes which are surrounded by a cement matrix. Due to the fact that construction aggregates are built from an arbitrary mix of sand, gravel, stones and recycled concrete of various shapes, it is feasible to assume the aggregates of a RVE to be spherical [26]. In reality, microcracks do not necessarily propagate uniformly in all directions since the crack tip growth is dictated by the superposition of static and dynamic stresses with inner stresses occurring as a result of ASR gel swelling, i.e. for a given stress application, there are always directions in which cracks are more likely to propagate. However, specific external stresses are not considered for the model in hand such that the assumption of uniformly distributed cracks is reasonable for the scope of this work.

Once formed within the aggregates, the ASR gel flows into the porous volume surrounding the aggregate and starts to exert pressure due to its swelling and continuosly increasing volume. The cracking of the surrounding matrix can be justified by the well-known fact that concrete has a much higher stiffness in compression than in tension. Figure 3.1 shows the structure of a RVE with differently sized aggregates.

The initially conforming crack surfaces roughen over time due to several chemo-mechanical

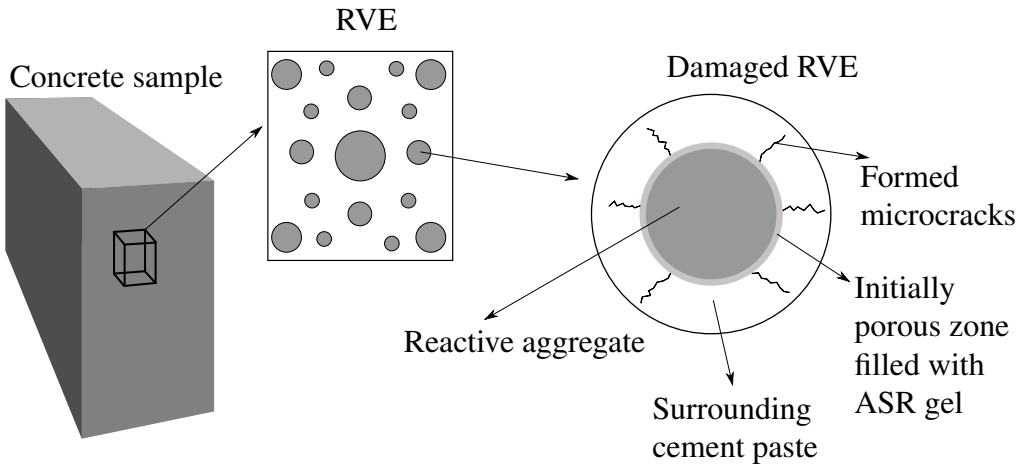

Figure 3.1: Schematic representation of representative volume element

processes such as grain detachment due to repeated rubbing or relative sliding motions of the crack surfaces. Consequently, the surfaces become non-conforming on a microscopic level, as shown in figure 3.2. Such a roughness is an inherent property of cracks in many types of solids [27]. The dashed line shows the original crack surface profile which can be approximated by equivalent spherical asperities when irregularities of smaller scales are neglected. The spherical asperities are located at different heights h and have sizes in the μm range. The overall three-dimensional crack contact area is a circle of radius R.

Since friction and shear sliding motions are neglected (see section 3.2), the nonlinearity of the crack stress depends only on the relative profile of the surfaces wherefore the elastic contact of two rough surfaces is replaced by the contact of a rigid flat surface with an elastic and rough composite surface containing the relative profile of the initial surfaces (figure 3.2). This is necessary because all distances between asperities need to be described using a single variable in order to obtain the complete crack nonlinearity by integrating over one variable. Moreover, the computational efficiency is improved compared to the case where the distance between each pair of asperities would need to be calculated separately.

A local coordinate system is assigned to each crack such that its origin is always fixed to the highest asperity with its z-axis pointing downward. The location and orientation

of each crack can then be linked to a fixed inertial coordinate system by an appropriate transformation law. Furthermore, this provides the ability to easily investigate differently oriented and distributed cracks by adjusting the distribution function and reintegrating over the concrete sample.

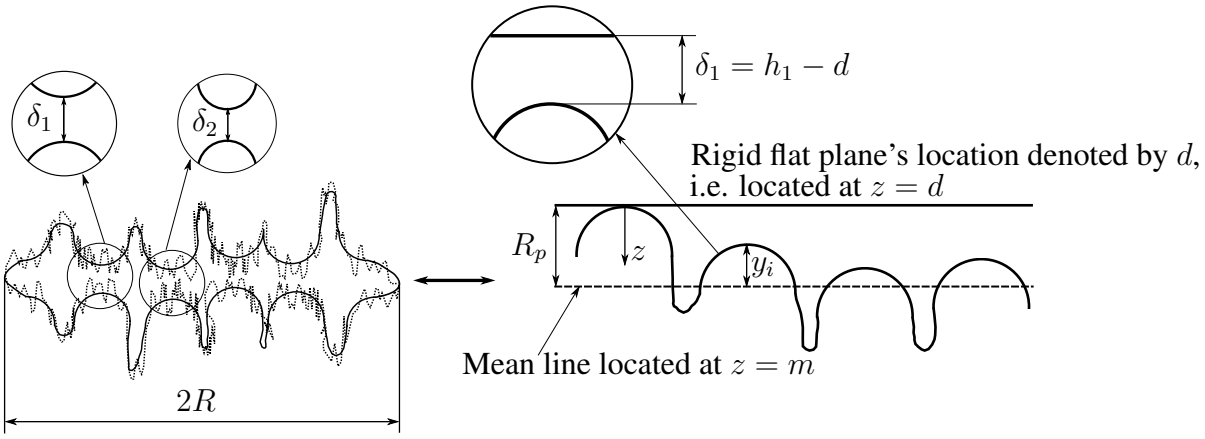

Figure 3.2: A schematic of the profile of two rough surfaces and the composite surface

On the right side of figure 3.2, the asperity profile is exaggerated along the z-axis for better depiction and therefore describes the crack in qualitative manner. In reality, the variation of asperity heights of the composite surface is lower that the asperity radius a (similar to left side of figure 3.2) and can be characterized by means of an algebraic sum of the two inital surfaces. For this purpose, a mean line is introduced at $z = m$ such that the volume between the mean line and the surface profile above the mean line equals to that below the mean line [28], $m = \frac{1}{n}\sum_{i=1}^{n} h_i$ where n and h_i are the number of asperities in the crack and the $z-$coordinate of the i-th asperity, respectively. Then, the root mean-squared roughness of the composite surface is given by

$$R_q = \sqrt{\frac{1}{n}\sum_{i=1}^{n}(y_i)^2} = \sqrt{\frac{1}{n}\sum_{i=1}^{n}(h_i - m)^2} = \sqrt{R_{q1}^2 + R_{q2}^2} \tag{3.1}$$

where y_i is the deviation in height of each asperity from the mean line, n is the total num-

ber of asperities and R_{q1} and R_{q2} represent the rms roughnesses of the two initial crack surfaces.

The variable d in figure 3.2 describes the location of the rigid flat. In order to obtain the nonlinear behavior of the crack during the approach, the rigid flat plane has to be moved towards the rough surface until it reaches the mean line and the respective stress within the crack is to be computed at each value for d. Due to the way the mean line has been defined, the rigid flat being at the mean line would imply a complete crack closure. The ultimate goal is therefore a mathematical description of all forces in terms of d and a subsequent integration over h from 0 to $m + R_p$, where $R_p = \max_i y_i$, for each value of d. Typical values for the microscopic rms roughness are examined in section 4.1.

3.2 Model assumptions

The exact motion of crack surfaces during an acoustic stress is a very complex process, specifically when the motion of a liquid between the surfaces is investigated in addition. For this reason, the model developed in this work is subject to several assumptions which make the problem easier to handle and implement into a numerical calculation tool. The main model assumptions are given below.

- The concrete around the cracks is assumed to have linear isotropic material properties, i.e. the entirety of aggregates, cement paste and ASR gel occurs uniformly in all directions. For a nonlinear elastic material, the analytical calculation of the stress in the surrounding solid would require FEM calculations. Volume or external forces other than the ones resulting from an acoustic stress are neglected such that the equilibrium equation $\boldsymbol{\nabla} \cdot \boldsymbol{P} = \mathbf{0}$ holds. Then, the stresses within a crack are balanced out by internal stresses in the surrounding solid in the case of a static equilibrium.

- Transverse sliding/shear motions do not occur. Therefore, a crack is stretched only under the action of a normal stress to the crack surface.

- The nonlinearity of a concrete sample originates from the nonlinearity of the cracks. Thus, the total strain is the sum of the strain of a perfectly linear elastic and homogeneous medium and the additional strain from cracks which is approximated by a Taylor series expansion up to the quadratic term.

- Each crack is penny-shaped, i.e. the crack opening area is a circle of radius R. The contact of two rough surfaces is transformed to the contact of a rigid flat plane with a rough elastic surface. Further, the crack concentration is sufficiently low to justify the negligence of crack interaction with other cracks. Specifically, the internal stress in the surrounding solid due to crack opening is determined separately for each crack.

- Inner pressure and swelling due to ASR gel generation within the aggregates and at the ITZ are neglected. The consideration of this process would be associated with a detailed description of the chemical process of ASR gel formation and liquid transport laws which is not within the scope of this work. The gel is rather assumed to be already present within the microcracks. Further information on ASR formation and transport can be found in [26].

- ASR gel is assumed to behave in a newtonian way, i.e. the viscous stress within the liquid is related linearly to the shear rate. Furthermore, its viscosity is low enough for the gel to flow aside without deforming the asperities which undergo an elastic deformation only due to mechanical contact stresses. Without this assumption, the use of the Hertzian contact approximation would not be suitable for this problem. However, concrete is usually a highly stiff material such that this assumption is justified.

- The lateral spacing between asperities is large enough to justify the negligence of ASR gel flow interaction between asperities. Section 3.3 shows that the ASR gel stays mainly in the area of its asperity, i.e. the extent to which an asperity is covered by gel during an approach does not exceed the asperity radius wherefore adjacent ASR gel ”blocks” do not exert pressure on one another. In this respect, the crack

radius R is assumed to be constant such that no crack growth occurs during crack closure due to increased stresses.

The assumption of cracks acting independently of each other is used often for low crack concentrations. In reality, there is an upper limit for the number of cracks for which the internal stresses in the surrounding solid can be computed separately. In order to investigate this limit, a sophisticated FEM model would be necessary to evaluate the exact interaction and how it affects the surrounding solid. Since the focus of this work is the assessment of nonlinearity change due to ASR gel, the assumption of low crack concentrations is essential.

3.3 Relationship between ASR gel volume and asperity wetting

In section 2.4.2, the lubrication force of ASR gel has been derived in terms of radial coordinates which describe the upper and lower limit of integration. In this section, these coordinates are linked to the amount of ASR gel and distance between the rigid flat plane and an asperity in order to enable the calculation of the lubrication force by prescribing a gel volume and a separation distance. The starting point for the derivation is qualitatively shown in figure 3.3 where two adjacent asperities partially covered by ASR gel are depicted.

In order to avoid absolute values, a relative volume ratio $V_{\mathrm{rel}} = \frac{V_{\mathrm{g}}}{V_{\mathrm{s}}}$ is prescribed to relate the gel volume over each asperity V_{g} to the volume of the asperity's semi-spherical top $V_{\mathrm{s}} = \frac{2}{3}\pi a^3$. Using the number of asperities in a crack n, the total gel volume within a crack $V_{\mathrm{g,tot}}$ can be obtained by $V_{\mathrm{g,tot}} = nV_{\mathrm{g}}$.

Each asperity, indexed by i, is located at a different height h_i from where its respective separation distance $\delta_i = h_i - d$ to the rigid flat can be computed for arbitrary values d. In figure 3.3, the separation of the left asperity $\delta_1 < 0$ since $h_1 = 0 < d$, i.e. the rigid flat has already deformed the asperity whereas on the right one, the separation distance $\delta_2 > 0$ is still positive for the depicted location of the rigid flat plane. The dashed part of the left

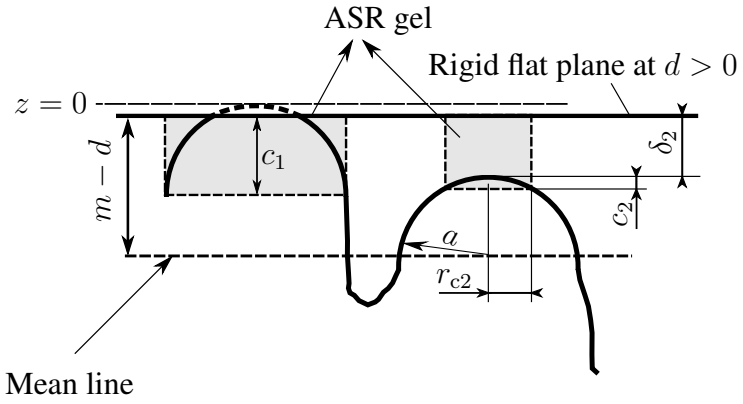

Figure 3.3: A schematic of a crack wetted by ASR gel

asperity shows the initially undeformed shape of the asperity top which is flattened due to the contact stress with the rigid plane. Ultimately, the aim is to compute the total crack pressure at any value for d, meaning that the expressions for all force components need to be written only in terms of d, V_{rel} and material constants.

It becomes evident that two different cases need to be considered separately when calculating the wetted portions of the tops in dependence on the gel amount, $\delta \geq 0$ and $\delta < 0$.

3.3.1 Separation distance $\delta \geq 0$

Due to its incompressibility, the gel is set in motion once the rigid flat plane is moved towards an asperity such that the asperity is immersed in gel to a bigger portion. The volume of the gel in the case of a positive separation distance δ is given by

$$V_{\mathrm{g}} = V_{\mathrm{rel}} V_{\mathrm{s}} = \pi \left[(r_c)^2 (\delta + c) - \frac{1}{3} c^2 (3a - c) \right] \tag{3.2}$$

The radial coordinate r_c at the sphere segment c can be computed by

$$r_c^2 + (a - c)^2 = a^2 \rightarrow r_c = \sqrt{c (2a - c)} \tag{3.3}$$

from where equation (3.2) becomes

$$V_{\mathrm{g}} = V_{\mathrm{rel}} V_{\mathrm{s}} = \pi \left[c\,(2a - c)\,(\delta + c) - \frac{1}{3} c^2\,(3a - c) \right] \tag{3.4}$$

This is a cubic equation for c from which a solution $c \in [0; a]$ is sought. There is a switch in two of the solutions at a certain relation between δ and c such that the sought one has to be determined using an if-condition on the value set of each solution in dependence on δ. This aspect is clarified at the end of this section with a plot of all solutions for c, highlighting the wanted one.

3.3.2 Separation distance $\delta < 0$

In the case of a negative separation distance, the calculation of the wetted portion is a little different since the deformed part of the sphere and the negative sign of δ have to be incorporated. The volume gel is then given by

$$V_{\mathrm{g}} = V_{\mathrm{rel}} V_{\mathrm{s}} = \pi \left[c\,(2a - c)\,(c - |\delta|) - \frac{1}{3} \left(c^2\,(3a - c) - \underbrace{|\delta|^2\,(3a - |\delta|)}_{\text{deformed sphere}} \right) \right] \tag{3.5}$$

As opposed to the gel, the spheres are not incompressible wherefore the dashed part of an asperity in figure 3.3 has to be subtracted from the total sphere volume as it is flattened by the rigid plane during the approach. Equation (3.5) is likewise a cubic equation from which the wanted solution for c at each d is obtained from Matlab. A closed form representation is omitted here due to its complexity.

Subsequently, an exemplary calculation of the wetted part of one asperity is performed to illustrate the transition of the cubic solutions. With this intention, the used parameters for the calculation are listed in table 3.1. The location of the asperity is chosen such that there is a sign change in the separation distance in the middle of the rigid flat's approach. The resulting plot is shown in figure 3.4.

Table 3.1: Parameters for calculation of asperity wetted portion

Parameter	**Value**
Asperity radius	$a = 5 \cdot 10^{-6}$ m
Relative volume ratio	$V_{\text{rel}} = 0.25$
Mean line location	$m = 1.2 \cdot 10^{-6}$ m
Asperity top location	$h = 0.6 \cdot 10^{-6}$ m

The solution for $\delta < 0$ is valid from the point where d exceeds the asperity top location h which happens at $d = 0.6 \cdot 10^{-6}$ m. For lower values of d, one of the two solutions for $\delta \geq 0$ is always negative and can be neglected. Using an if-condition, the transition point can be found where the used value for the determination of force components is switched from the first to the second solution. The eventual values for the wetted portion, partially composed of different solutions to the cubic equations, are represented by the black dashed line in figure 3.4.

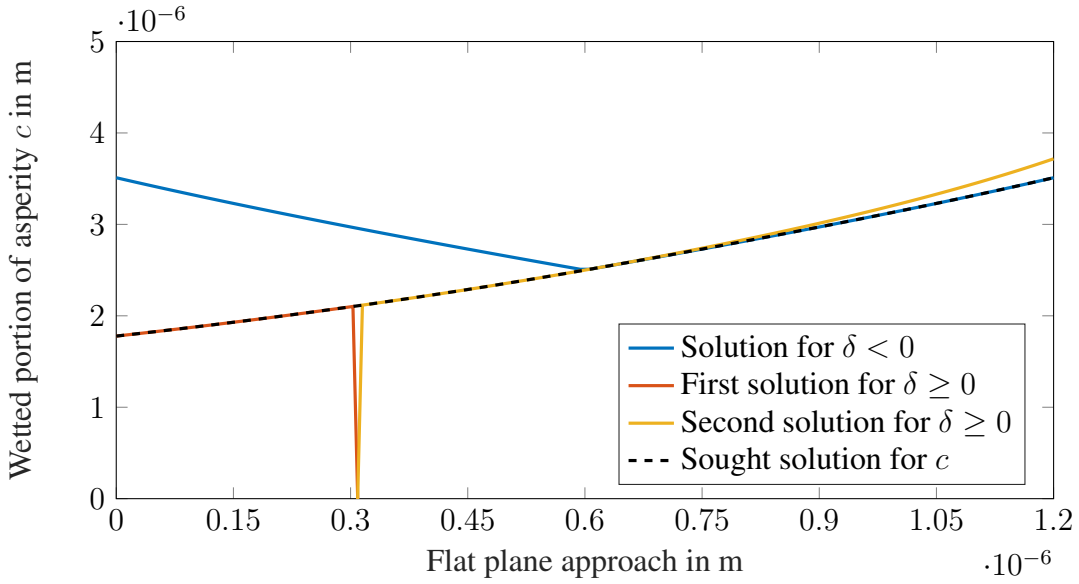

Figure 3.4: Calculation of wetted portion c in dependence on separation distance δ and volume ratio V_{rel}

The y-axis in figure 3.4 is limited from 0 to the asperity radius a for a better classi-

fication of the wetted portion c compared to the asperity radius. It is visible that even at the highest approach value for d where the flat plane reaches the mean line of the crack surface, the wetted portion is still lower than the asperity radius which means that even if two asperities were located right next to each other, touching one another at a point, the gel amounts over each asperity would not come in lateral contact. This justifies the negligence of lateral interaction of adjacent ASR gel "blocks". It is worth noting that the shown volume ratio of $V_{\mathrm{rel}} = 0.25$ is just about the upper limit for this parameter and will be justified in the further course of this work when the crack volume is adressed.

An interesting observation on the slope of the sought solution can be made by comparing the courses of the yellow and blue line. The fact that the blue line has a more linear course than the yellow one can be explained by the fact that it is valid at higher z-values where half of the asperity is already covered in gel (y-value in figure 3.4 at $d \geq 0.6 \cdot 10^{-6}$ m). From this point, the surface of the asperity takes a steeper course in the z-direction, making the relation between d and c more linear whereas for lower values of d, c increases nonlinearly due to the higher $\frac{\partial r_c}{\partial c}$.

Now that equations (3.4) and (3.5) can be solved numerically for $c(V_{\mathrm{g}}, d)$ once a desired gel volume ratio is prescribed, the force components acting on each asperity can be computed taking into account the asperity's location and thus its clearance to the rigid flat plane.

3.4 Forces acting on a pair of asperities

For the purpose of calculating the overall crack pressure, the total force acting on each asperity needs to be known in terms of the gel volume and separation distance δ. Hence, this section provides complete expressions for all force components and highlights their differences before and after a respective asperity has come into contact with the rigid flat. In chapter 2, the lubrication and contact force have been derived in a general manner and are specified more precisely here. The total force acting between the asperity i and the rigid

flat is composed as follows.

$$F_i = \begin{cases} F_{i,\delta\geq 0} = F_{\mathrm{L},\,\delta\geq 0} & \text{for} \quad \delta \geq 0 \rightarrow h_i \geq d \\ F_{i,\delta<0} = F_{\mathrm{L},\,\delta<0} + F_{\mathrm{c}} & \text{for} \quad \delta < 0 \rightarrow h_i < d \end{cases}$$

where F_{L} represents the lubrication force which can be thought of as an inner resistance force of the gel against flow and F_{c} is the contact force due to elastic deformation.

The numerical solutions of equations (3.4) and (3.5) for $c(V_{\mathrm{g}}, d)$ are noted by $c_{\delta\geq 0}$ and $c_{\delta<0}$ in the following. Since they are solved for in a numerical way in Matlab, exact analytical expressions of reasonable length can not be obtained. It should be noted that they are not independent variables but rather depend on V_{rel} and d directly.

Using this, precised expressions for the total force can be derived. Starting with the case $\delta \geq 0$ and substituting equation (3.4) into equation (2.38), one obtains

$$\begin{aligned} F_i = \frac{2\pi\mu_{\mathrm{L}} a^2 v}{6b^2} \Bigg[& 6b \ln\left(1 + \frac{c_{\delta_i\geq 0}\,(2a - c_{\delta_i\geq 0})}{2a\delta_i}\right) + \frac{c_{\delta_i\geq 0}\,(2a - c_{\delta_i\geq 0})}{2a} + (6b + \delta_i)\ln(6b + \delta_i) \\ & - \left(6b + \delta_i + \frac{c_{\delta_i\geq 0}\,(2a - c_{\delta_i\geq 0})}{2a}\right)\ln\left(6b + \delta_i + \frac{c_{\delta_i\geq 0}\,(2a - c_{\delta_i\geq 0})}{2a}\right) - \delta_i\,(\ln(\delta_i) - 1) \\ & + \left(\delta_i + \frac{c_{\delta_i\geq 0}\,(2a - c_{\delta_i\geq 0})}{2a}\right)\left(\ln\left(\delta_i + \frac{c_{\delta_i\geq 0}\,(2a - c_{\delta_i\geq 0})}{2a}\right) - 1\right)\Bigg] \end{aligned} \tag{3.6}$$

whereas in the case of a negative δ, the force is given by substituting equation (3.5) into

equation (2.40):

$$F_i = \frac{2\pi\mu_{\mathrm{L}}a^2v}{6b^2}\Bigg[6b\ln\left(\frac{2a|\delta_i| + c_{\delta<0}\left(2a - c_{\delta<0}\right)}{2a|\delta_i| + |\delta_i|\left(2a - |\delta_i|\right)}\right) - \frac{|\delta_i|\left(2a - |\delta_i|\right) - c_{\delta<0}\left(2a - c_{\delta<0}\right)}{2a}$$
$$- \left(6b + |\delta_i| + \frac{c_{\delta<0}\left(2a - c_{\delta<0}\right)}{2a}\right)\ln\left(6b + |\delta_i| + \frac{c_{\delta<0}\left(2a - c_{\delta<0}\right)}{2a}\right)$$
$$+ \left(6b + |\delta_i| + \frac{|\delta_i|\left(2a - |\delta_i|\right)}{2a}\right)\ln\left(6b + |\delta_i| + \frac{|\delta_i|\left(2a - |\delta_i|\right)}{2a}\right)$$
$$+ \left(|\delta_i| + \frac{c_{\delta<0}\left(2a - c_{\delta<0}\right)}{2a}\right)\left(\ln\left(|\delta_i| + \frac{c_{\delta<0}\left(2a - c_{\delta<0}\right)}{2a}\right) - 1\right)$$
$$- \left(|\delta_i| + \frac{|\delta_i|\left(2a - |\delta_i|\right)}{2a}\right)\left(\ln\left(|\delta_i| + \frac{|\delta_i|\left(2a - |\delta_i|\right)}{2a}\right) - 1\right)\Bigg] + \frac{4}{3}\frac{E}{2\left(1-\nu^2\right)}a^{\frac{1}{2}}\,|\delta|^{\frac{3}{2}} \tag{3.7}$$

Equations (3.6) and (3.7) describe the force acting on a single pair of oppositely located asperities. In order to calculate the pressure within the whole crack, an appropriate top height distribution function is required which describes the number of asperities and their location along the z-axis per unit area. Subsequently, the obtained functions have to be integrated over h within the limits of the asperity height distribution. This aspect is adressed in the following.

3.5 Asperity height distribution functions and crack pressure

The spatial variation, that is the variation in heights of asperity tops, plays a significant role in a crack nonlinearity analysis. Therefore, a statistical distribution $\phi(z)$ in the form of a probability density function is required in order to distribute the heights of asperities h_i over $[0; m + R_p]$. Many surfaces have been shown to be liable to symmetrical distributions [29] and can be represented by the widely used Gaussian distribution, wherefore at least one of the central moments needs to be known in addition to the mean value m. The first

central moment is called the variance

$$\mathrm{Var}(h) = \sum_{i=1}^{n} \phi_i \left(h_i - m\right)^2 = \frac{1}{n} \sum_{i=1}^{n} \left(h_i - m\right)^2 \tag{3.8}$$

whereas the second one

$$\sigma = \sqrt{\mathrm{Var}(h)} = \sqrt{\frac{1}{n} \sum_{i=1}^{n} \left(h_i - m\right)^2} \tag{3.9}$$

is referred to as standard deviation and is more common in the description of surface textures since it is formally equal to the rms roughness R_q. The central moments in general provide a measure of the range over which the values are spread. Based on the maximum peak value R_p measured from the mean line m, the standard deviation can be chosen as

$$\sigma = \frac{1}{3} R_p \tag{3.10}$$

in order to ensure that $99.7\,\%$ of all peaks are located in the range $[0; m + R_p]$. Then, the Gaussian distribution can be written as

$$\phi_{\mathrm{G}}(h) = \frac{1}{\sigma\sqrt{2\pi}} exp\left(-\frac{\left(h - m\right)^2}{2\sigma^2}\right) \tag{3.11}$$

The exact height distribution of asperities depends significantly on the aggregates shape and their grains since microcracks typically propagate along the these as shown in figure 3.5.

As mentioned before, aggregates can be located randomly and have various shapes wherefore another asperity height distributions should be taken into consideration as well. In fact, [6] employs an exponential distribution of the form

$$\phi_{\mathrm{E}}(h) = \lambda_{\mathrm{E}}\, exp\left(-\lambda_{\mathrm{E}} h\right) \tag{3.12}$$

where $\lambda_{\mathrm{E}} = 1 \setminus \sigma$ is called the rate parameter. The influence of ϕ on the change of nonlin-

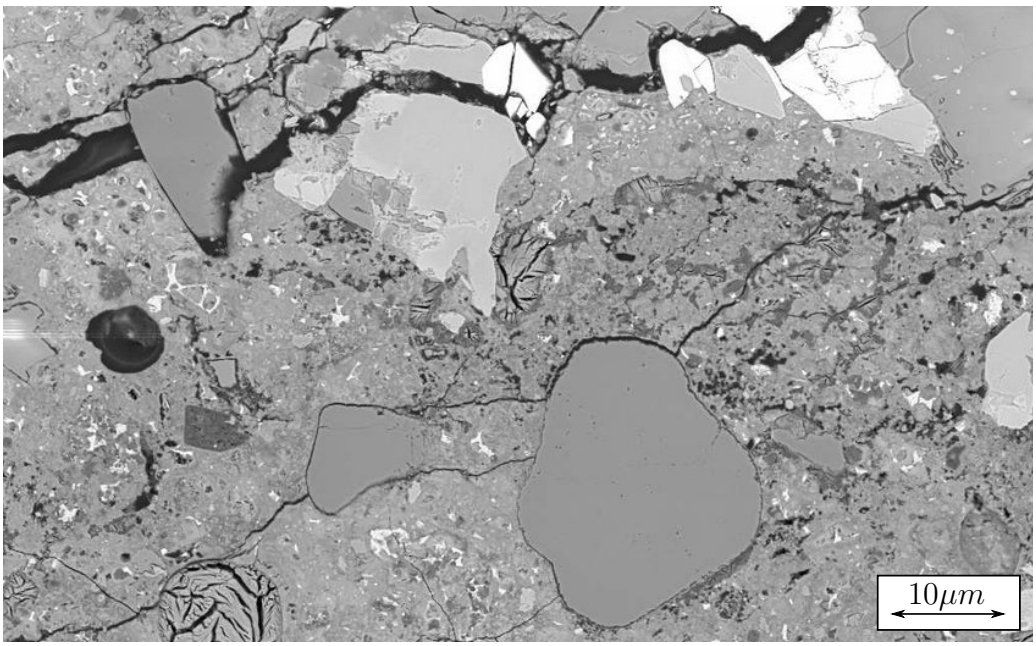

Figure 3.5: Typical image of a microcrack in a concrete structure [30]

earity is therefore one of the aspects investigated in section 4.1.

Once an appropriate distribution function has been chosen, the stress within the crack can be obtained by integrating over the whole range of h. For the analysis in hand, the integral needs to be split in two parts: one accounting for non-negative values for δ and one accounting for negative values. The two parts mainly differ in the force expressions and integration limits for h. With this in mind, the pressure within the crack is written as

$$p(d) = \overline{n} \int_0^d F_{\delta<0}\left(h-d\right)\phi(h)dh + \overline{n} \int_d^{m+R_p} F_{\delta\geq 0}\left(h-d\right)\phi(h)dh \tag{3.13}$$

where $\overline{n} = \frac{n}{\pi R^2}$ with $n = \zeta \frac{R^2}{a^2}$ being the number of asperities in the entire crack which is scaled to an unit of area in $\overline{n}$. ζ represents a spacing variable $\zeta \in [0;1]$ which is a measure for the lateral clearance between asperities (for $\zeta = 1$ all asperities are located right next to each other). The unit of $\overline{n}$ then becomes m^{-2} and together with the force component, the required unit for stress is obtained.

The expression given in equation (3.13) can not be solved in analytically. For this reason, the computation is conducted in Matlab where a relative tolerance of 3% is accepted for the numerical integration due to the significantly reduced computational effort (results are obtained within less than a minute). For comparison purposes, it is worth noting than the computation with a relative tolerance of 10^{-6} (default value in Matlab) requires approximately 20 minutes to yield a pressure result.

In the following, an exemplary calculation of the pressure within a crack is conducted and plotted over the location of the rigid flat plane in figure 3.6. The used parameters for the calculation are listed below whereby their exact composition is addressed in the next chapter.

Table 3.2: Parameters for calculation of crack pressure

Parameter	**Value**
Asperity radius	$a = 7 \cdot 10^{-6}$ m
Relative volume ratios	$V_{\mathrm{rel}} \in [0; 0.3]$
Mean line location	$m = 1.2 \cdot 10^{-6}$ m
Crack radius	$R = 10^{-4}$ m
El. constants of concrete	$E = 32.517$ GPa and $\nu = 0.231$
Maximum asperity height variation	$R_p = 1.2 \cdot 10^{-6}$ m
rms roughness, standard deviation	$\sigma = 4 \cdot 10^{-7}$ m
Asperity top height distribution	Gaussian
Slip Length	$b = \mu_{\mathrm{L}}^{0.65}$ m

The blue line shows the stress due to pure mechanical contact. The total area of contact increases with the flat plane approach wherefore the stiffness $\partial p/\partial d$ incrementally increases. This course of the contact pressure between rough surfaces is well known and can be found in several works [31, 32]. An alternative illustration can be obtained by reversing the axes such that the normal stress represents the $x-$axis, leading to a degressive course of the lines, i.e. the required normal stress increases towards crack closure.

Due to the increasing stiffness, the pressure graph is highly nonlinear. The remaining lines represent the pressure in the crack including the effect of ASR gel. Since a resistance

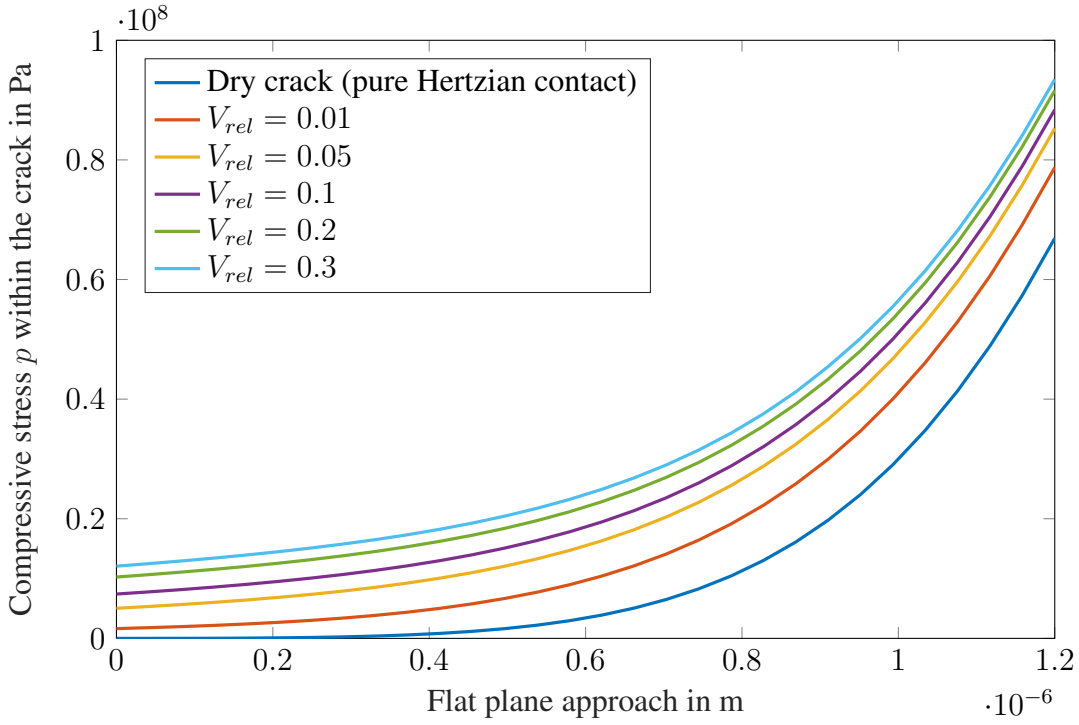

Figure 3.6: Calculation of crack pressure p in dependence on flat plane approach d and volume ratio V_{rel}

due to liquid viscosity occurs already before mechanical contact, the graphs tend to reduce in terms of nonlinearity as the gel amount increases. As the flat wall approaches the middle line, the shown graphs become parallel since the Hertzian contact becomes the leading term in the pressure equation.

The main focus of this thesis is to examine the reduction of nonlinearity due to presence of ASR gel. For this purpose, an equilibrium equation including all pressure terms is required. In a static case, the pressure within the crack is compensated by an internal stress in the surrounding solid, leading to an equilibrium crack opening at which both stresses are equal in magnitude and act in opposite directions. Under the action of an additional acoustic stress $\tilde{p}(\tilde{d})$, the solid's equilibrium needs to be adjusted by incorporating the effect of the acoustic stress. Subsequently, an expression for $\tilde{p}(\tilde{d})$ is sought which can be then compared to equation (2.13) in order to obtain the nonlinearity in dependence on the gel

volume.

3.6 Crack equilibrium opening and nonlinearity

The exact value of the internal stress in the close proximity of the rough crack contains local variations due to roughness which can not be determined easily wherefore the stress p_0 has been calculated based on a penny shaped crack for which an analytical formula exists. In order to establish a relation between p and p_0, an assumption of volume equality of a penny shaped crack and the rough crack has to be adopted although their shapes differ slightly [6]. Using this, the static equilibrium of the solid can be written as

$$p\left(V_{\text{rel}}, d_0\right) = p_0\left(d_0\right)$$

$$\overline{n}\left[\int_0^{d_0} F_{\delta<0}\left(h-d_0\right)\phi(h)dh + \int_{d_0}^{m+R_p} F_{\delta\geq 0}\left(h-d_0\right)\phi(h)dh\right] = \frac{3E\pi(R_p-d_0)}{16\left(1-\nu^2\right)R} \quad (3.14)$$

from where $d_0\left(V_{\text{rel}}\right)$ can be obtained numerically for each gel volume ratio (figure 3.7). The graphs on the left plot have the same meaning as in figure 3.6.

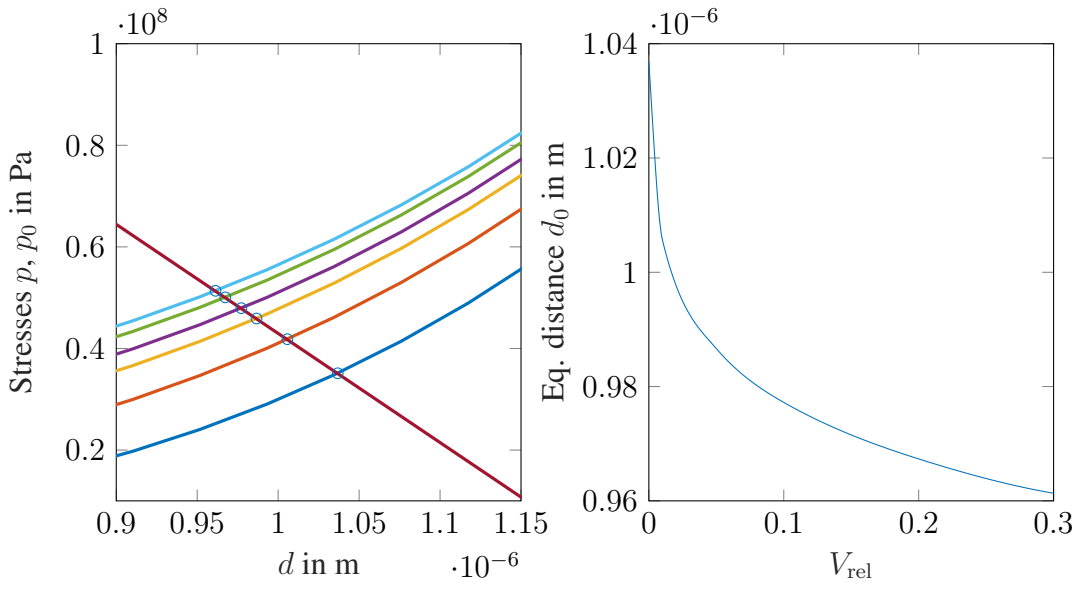

Figure 3.7: Equilibrium between p_0 and p for different V_{rel}, same legend as in figure 3.6

The dry crack provides the least resistance against the internal stress in the solid in close proximity to the crack wherefore the flat plane has the highest equilibrium value when compared to partially filled cracks. It is worth recalling that increasing values for d describe crack closure since the flat is moved towards the rough surface, i.e. the dry crack has the lowest equilibrium opening. The circles on the left plot show at which value for d the two oppositely directed stress components are equal in magnitude. On the right side, the equilibrium opening is plotted over the amount of ASR gel, showing a significantly larger crack opening for a gel volume ratio of 0.3 compared to a dry crack.

In the following, an acoustic pressure wave propagating normal to the crack opening and causing a displacement of the rigid plane location $\tilde{d}$, as shown schematically in figure 3.8, is considered.

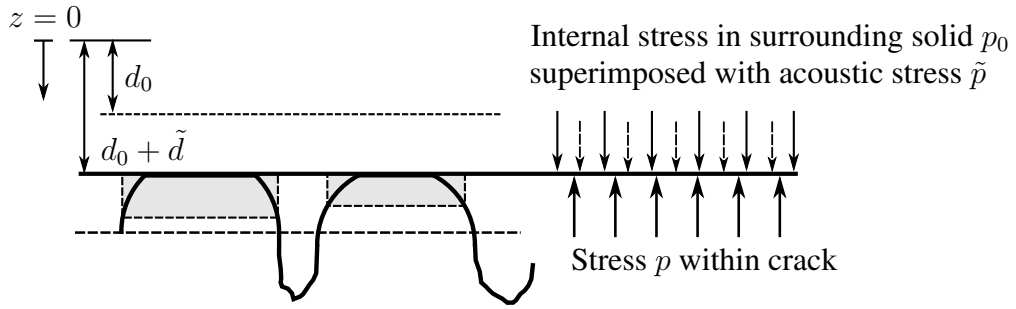

Figure 3.8: Sketch of the solid's dynamic equilibrium

In order to displace the rigid wall by $\tilde{d}$, the wave has to cause an acoustic pressure $\tilde{p}$ which equals to the pressure difference between p and p_0. Formally, the dynamic equilibrium of the solid can be written as

$$\tilde{p}(\tilde{d}) = p_0(d_0 + \tilde{d}) - p(d_0 + \tilde{d}) \tag{3.15}$$

In the case of a positive $\tilde{d}$, the magnitude of p becomes larger than p_1 but since p points in the negative z direction, the acoustic pressure $\tilde{p}$ turns positive which is necessary in order

to displace the rigid wall in the positive z direction. Graphically, the magnitude of $\tilde{p}$ is illustrated in figure 3.9 for a negative $\tilde{d}$. It is apparent that $\tilde{p}$ is composed of a linear and a nonlinear stress component, meaning that the function for the acoustic stress is of nonlinear nature. For the purpose of a nonlinearity investigation of an entire solid (next chapter), the crack opening variation $\tilde{d}$ needs to be expressed in terms of the acoustic stress, i.e. $\tilde{d}(\tilde{p}, \tilde{p}^2)$. The reason behind this conversion is that the total strain of a solid can be written as the sum of a perfectly linear, homogeneous strain and the additional strain due to crack opening which can be deduced from the opening displacement. Eventually, the total strain will be obtained as a nonlinear function of the acoustic stress.

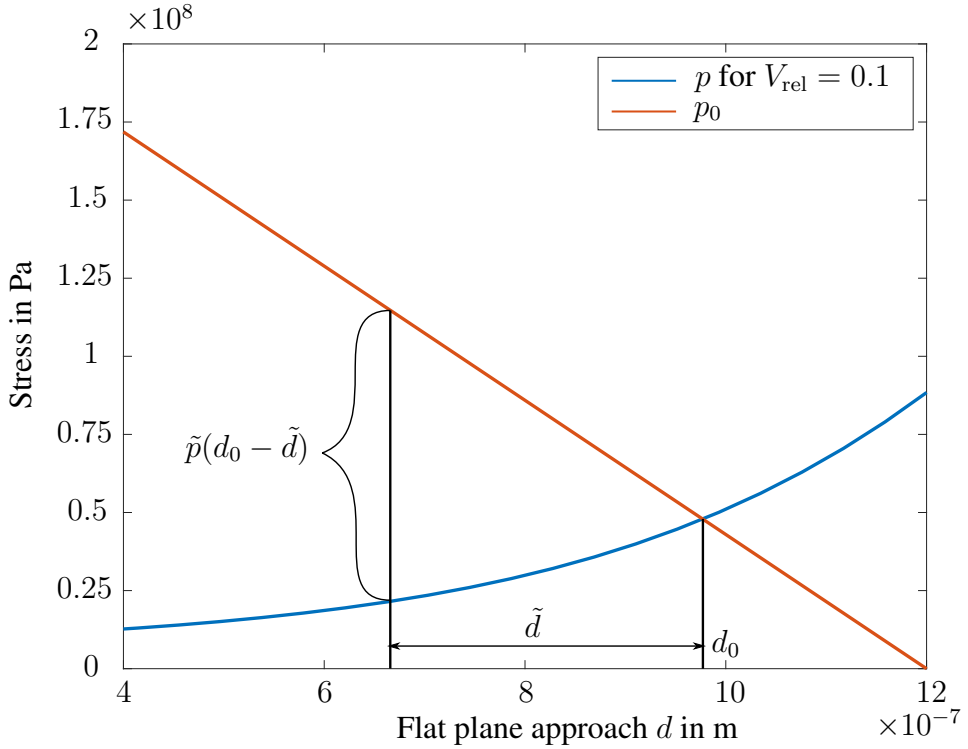

Figure 3.9: Graphic representation of $\tilde{p}(\tilde{d})$

The normal displacement $\tilde{d}$

$$\tilde{d} = d - d_0(V_{\text{rel}}) \tag{3.16}$$

is dependent on V_{rel} for a desired position of the flat plane d due to the varying equilibrium

distances $d_0(V_{\mathrm{rel}})$.

Since the results were obtained numerically (due to the complexity of the stress within the crack), an appropriate way to yield values for the nonlinearity is fitting a nonlinear curve up to the quadratic term for every gel amount. Therefore, Matlab's built-in "cftool" is used based on the method of least squares where the summed squares of all residuals are minimized. The fitted equation has the form of a Taylor expansion

$$\tilde{d} = \alpha_{\mathrm{cr}}\,\tilde{p} + \frac{1}{2}\beta_{\mathrm{cr}}\,\tilde{p}^2 \tag{3.17}$$

where a constant term does not occur because the acoustic stress has been defined such that it equals zero at equilibrium ($\tilde{d} = 0$). Equation (3.17) is used in the next section to derive the total strain of a cracked solid.

3.7 Averaged nonlinearity with respect to crack orientation and distribution

The preceeding sections were concerned with the derivation of the nonlinearity of a single crack with respect to its local coordinate system where the z axis is always located normal to the crack opening surface. In reality, considerably more interesting is the nonlinearity of an entire solid due to the fact that a single crack is never measured in the scope of non-destructive evaluation. The current NDE techniques allow the installation of a transducer and receiver on a solid's surface wherefore the nonlinearity is obtained as an averaged parameter over the body. For this reason, the crack nonlinearity needs to be extended to a cracked medium with various cracks of different orientations and locations by using an appropriate averaging scheme.

Figure 3.10 shows a crack within the representative volume element which is first rotated about the global Y axis by an angle θ (front view). On the left side of figure 3.10, the crack is still located in the $X - Z$ plane and the circular opening appears as a straight line. Subsequently, the crack is rotated by an angle ψ about the global Z axis such that the

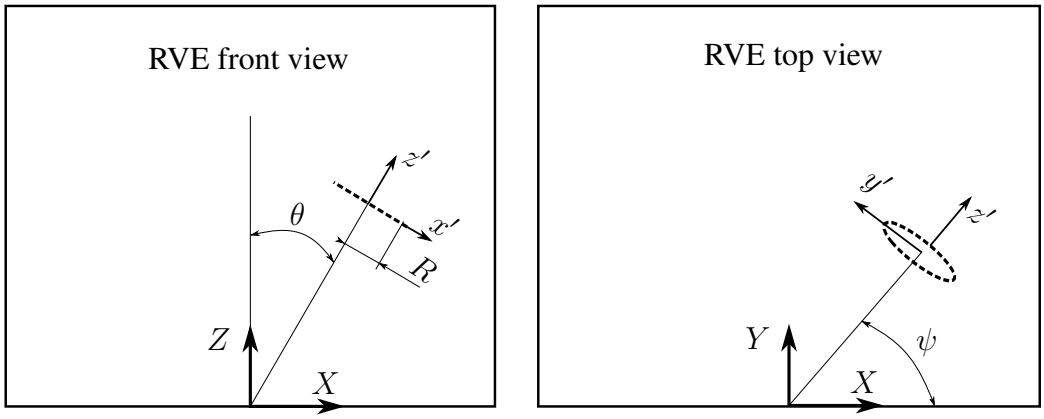

Figure 3.10: RVE: relation between local and global coordinate system

projection of the local z axis on the $X-Y$ plane makes the angle ψ with the X axis.

The tensor transformation law is given by

$$S_{ij} = Q_{ip}Q_{jq}S'_{pq} = Q_{ip}S'_{pq}Q_{qj} \tag{3.18}$$

where

$$Q_{ip} = e_i \cdot e'_j = \begin{bmatrix} cos(\theta)cos(\psi) & -sin(\psi) & sin(\theta)cos(\psi) \\ cos(\theta)sin(\psi) & cos(\psi) & sin(\theta)sin(\psi) \\ -sin(\theta) & 0 & cos(\theta) \end{bmatrix} \tag{3.19}$$

with e_i being the i-th basis unit vector of the global coordinate system. Therefore, a local normal strain ϵ'_{zz} causes the following normal strains in the global frame.

$$\epsilon_{xx} = sin^2(\theta)\, cos^2(\psi)\, \epsilon'_{zz}$$

$$\epsilon_{yy} = sin^2(\theta)\, sin^2(\psi)\, \epsilon'_{zz}$$

$$\epsilon_{zz} = cos^2(\theta)\, \epsilon'_{zz} \tag{3.20}$$

For a 1D pressure wave which is approximated with an elastic half space, the nonlinearity parameter β relates the stress to the quadratic strain component in the stress direction wherefore only one term of the strain tensor has to be considered when the nonlinearity of a cracked medium is derived.

According to Pecorari [33], the constitutive relationship of a cracked medium can be written as

$$\epsilon_{ij} = S_{ijkl} P_{kl} + \frac{1}{2V} \sum_r \left[\tilde{d}_i n_j + \tilde{d}_j n_i \right]^r A^r \tag{3.21}$$

where S_{ijkl} is the compliance tensor of the non-cracked medium, n_i is the i-th component of a unit vector normal to a crack's surface and $\tilde{d}_i$ is the i-th component of the crack opening displacement. V describes the volume of the RVE and A^r its surface area with r being a countering index for cracks. For an one-dimensional pressure wave which propagates and displaces along the z direction and causes a stress $P_{ij} = \delta_{iz}\tilde{p}$, the respective strain becomes

$$\epsilon_{zz} = S_{zzzz} P_{zz} + \frac{1}{V} \sum_r \left[\tilde{d}_z n_z \right]^r A^r \tag{3.22}$$

Substituting equation (3.17) for $\tilde{d}$ and transforming the equations to the global coordinate system yields

$$\epsilon_{zz} = \frac{1}{E}\tilde{p} + \frac{1}{V} \sum_r \left[cos^2(\theta) \left(\alpha_{\mathrm{cr}}\, cos^2(\theta)\, \tilde{p} + \frac{1}{2}\beta_{\mathrm{cr}}\, cos^4(\theta)\, \tilde{p}^2 \right) \right]^r A^r \tag{3.23}$$

The $cos^2(\theta)$ term in front of the expression for $\tilde{d}$ originates from the transformation of $\tilde{d}$ and n_z. The pressure $\tilde{p}$ was defined to act normal to the crack surface and therefore has to be transformed respectively in this equation as well. Rearranging the terms with respect to

the powers of $\tilde{p}$ leads to

$$\epsilon_{zz} = \left[\frac{1}{E} + \frac{1}{V}\sum_r \alpha_{\mathrm{cr}}\, cos^4\left(\theta\right) A^r\right]\tilde{p} + \frac{1}{2V}\sum_r \beta_{\mathrm{cr}}\, cos^6\left(\theta\right) A^r \tilde{p}^2 \tag{3.24}$$

It becomes clear that for a 1D wave acting along the z-direction, the orientation relative to the x- axis, described by ψ, has no effect on the nonlinearity. This also makes sense since the crack opening is only dictated by the orientation of the crack to the z- axis, i.e. its opening would be the same for any ψ. If other types of nonlinearity were to be analyzed (e.g. transverse nonlinearity β_{T} with a shear wave), then the orientation given by ψ would be important as it characterizes if the additional strain due to crack opening is along the x or y axis.

Moreover, in section 3.1 an assumption of equal crack propagation with respect to direction has been made. In a real application, the inner swelling of ASR gel would have to be superimposed with externally applied stresses (i.e. stress due to weight, vehicles driving over a bridge etc) and the overall direction of highest shear stress would be more likely for cracks to propagate in. Since the work in hand is not based on a certain application, the cracks can be oriented equally in all directions and the sum of cracks can be written as

$$\begin{aligned}
\frac{1}{V}\sum_r \alpha_{\mathrm{cr}}\, cos^4\left(\theta\right) A^r &= N_0\, \alpha_{\mathrm{cr}}\, cos^4\left(\theta_{\mathrm{avg}}\right) \pi R_{\mathrm{avg}}^2 \\
\frac{1}{V}\sum_r \beta_{\mathrm{cr}}\, cos^6\left(\theta\right) A^r &= N_0\, \beta_{\mathrm{cr}}\, cos^6\left(\theta_{\mathrm{avg}}\right) \pi R_{\mathrm{avg}}^2
\end{aligned} \tag{3.25}$$

with N_0 being the crack density in $1/m^3$. It should be noted that the crack radius R is a variable which follows a distribution function depending on time. For simplicity, a uniform distribution with an average crack radius R_{avg} is used here. Then, the linear and nonlinear

compliances of a cracked medium can be obtained as

$$S_{\mathrm{L}} = \frac{1}{E} + N_0 \alpha_{\mathrm{cr}}\, cos^4\left(\theta_{\mathrm{avg}}\right) \pi R_{\mathrm{avg}}^2$$
$$S_{\mathrm{N}} = \frac{N_0}{2} \beta_{\mathrm{cr}}\, cos^6\left(\theta_{\mathrm{avg}}\right) \pi R_{\mathrm{avg}}^2 \tag{3.26}$$

In order to calculate the linear and nonlinear elastic constants of stiffness, a series reversion needs to be performed.

$$C_{\mathrm{L}} = \frac{1}{S_{\mathrm{L}}} = \frac{E}{1 + E N_0\, \alpha_{\mathrm{cr}}\, cos^4\left(\theta_{\mathrm{avg}}\right) \pi R_{\mathrm{avg}}^2}$$
$$C_{\mathrm{N}} = -\frac{S_{\mathrm{N}}}{S_{\mathrm{L}}^3} = \frac{\frac{N_0}{2} \beta_{\mathrm{cr}}\, cos^6\left(\theta_{\mathrm{avg}}\right) \pi R_{\mathrm{avg}}^2}{\left(\frac{1}{E} + N_0 \alpha_{\mathrm{cr}}\, cos^4\left(\theta_{\mathrm{avg}}\right) \pi R_{\mathrm{avg}}^2\right)^3} \tag{3.27}$$

The given constants have the unit Pa. In order to extract a dimensionless β, as shown in equation (2.13), C_{L} and C_{N} are divided by $\lambda + 2\mu$, leading to

$$P_{zz} = (\lambda + 2\mu) \left[\frac{C_{\mathrm{L}}}{\lambda + 2\mu} \epsilon_{zz} + \frac{1}{2} \frac{C_{\mathrm{N}}}{(\lambda + 2\mu)} \epsilon_{zz}^2 \right] \tag{3.28}$$

Since a $1D$ wave propagation is well approximated by an elastic half space with no transversal strain, $\lambda + 2\mu$ equals E (Poisson's ratio $\nu = 0$) such that in the case of $N_0 = 0$, the linear elastic case $P_{zz} = (\lambda + 2\mu)\, \epsilon_{zz}$ is recovered.

CHAPTER 4
PARAMETRIC STUDY AND SIMULATION

In the first part of this chapter, a parametric study is conducted with the main parameters of the model. Second, simulation results are shown for different crack sizes and crack densities in order to analyze the relative and total nonlinearity change due to growing cracks.

4.1 Parametric study

The physical model introduced in chapter 3 depends on several parameters for which a sensitivity analysis needs to be performed towards ascertaining the influence of different parameters on the overall nonlinearity results. To do so, suitable ranges need to be determined based on results provided by other works. Afterwards, simulation results are plotted over the determined ranges to show the nonlinearity change.

4.1.1 ASR gel viscosity

One of the most important constants on which the model is based is the viscosity of ASR gel since it dictates the resistance against flow and thus the lubrication force. The chemical composition of ASR gel varies, characterized by the amounts of alkali, alkaline earth oxides (sodium, potassium and calcium oxides), silica and water in the concrete. The general composition of ASR gel can be represented as $(SiO_2)(CaO)_c(Na_2O)_n(K_2O)_k(H_2O)_x$ where c, n, k and x are time-dependent molar ratios. Vayghan [34] synthesized specimens with various ASR gel compositions and measured their elastic properties as well as stress-strain results over time in order to calculate the viscoelastic parameters of ASR gel using a Burger's model. In such a model, the viscosity of a liquid is composed of an instantaneous and a long-term viscosity. Due to the high velocities of a pressure wave, the instantaneous part is leading for the application in hand. According to his dissertation results, the gel viscosity

ranges as

$$3.92 \cdot 10^8 Pa \cdot s \leq \mu_{\mathrm{L}} \leq 3.41 \cdot 10^{12} Pa \cdot s \tag{4.1}$$

Moreover, the shear stress at the asperity surface can be described as

$$\tau_{\mathrm{s}} = k v_r^{(\mathrm{s})} = \mu_{\mathrm{L}} \frac{\partial v_r}{\partial z}\bigg|_{z=\delta} = \mu_{\mathrm{L}} \frac{v_r^{(\mathrm{s})}}{b} \tag{4.2}$$

where k represents the friction coefficient at the solid's surface. From equation (4.2), it can be seen that for Newtonian fluids, the gel viscosity μ_{L} is given by the product of the slip length b and the friction coefficient k. Since both these quantities depend on the gel viscosity, it should be possible to write these in terms of μ_{L}. However, an exact determination would require solving a discrete model which involves partial differential equations because the slip and thus the gel velocity might vary with time and space. Since this is not in the scope of this work, an estimation needs to be made wherefore the slip length is written as

$$b = \mu_{\mathrm{L}}^x, \qquad 0 \leq x \leq 1 \tag{4.3}$$

where $x = 0.65$ was found to yield a smooth transition from positive to negative separation distances. As mentioned in [34], the gel viscosity is highly dependent on the chemical composition, i.e. proper knowledge of the gel composite is necessary in order to estimate the nonlinearity accurately. Figure 4.1 shows the pressure p over relative approach d inside a crack for two low amounts of ASR gel at varying gel viscosities. It is visible that μ_{L} has an important effect on the pressure course. On the right side of figure 4.1, the effect is more pronounced due to the higher total amount of gel present in the crack. For a comparison of the nonlinearity decrease, β_{N} has been calculated and plotted over the gel viscosity and over the gel volume in figure 4.2. Note that β_{N} is a dimensionless and normalized parameter (divided by the nonlinearity of a dry crack). In compliance with figure 4.1, figure 4.2 shows a continuously decreasing nonlinearity with increasing gel volumes. For the highest investigated value of μ_{L}, the nonlinearity decreases to approximately 74%. For

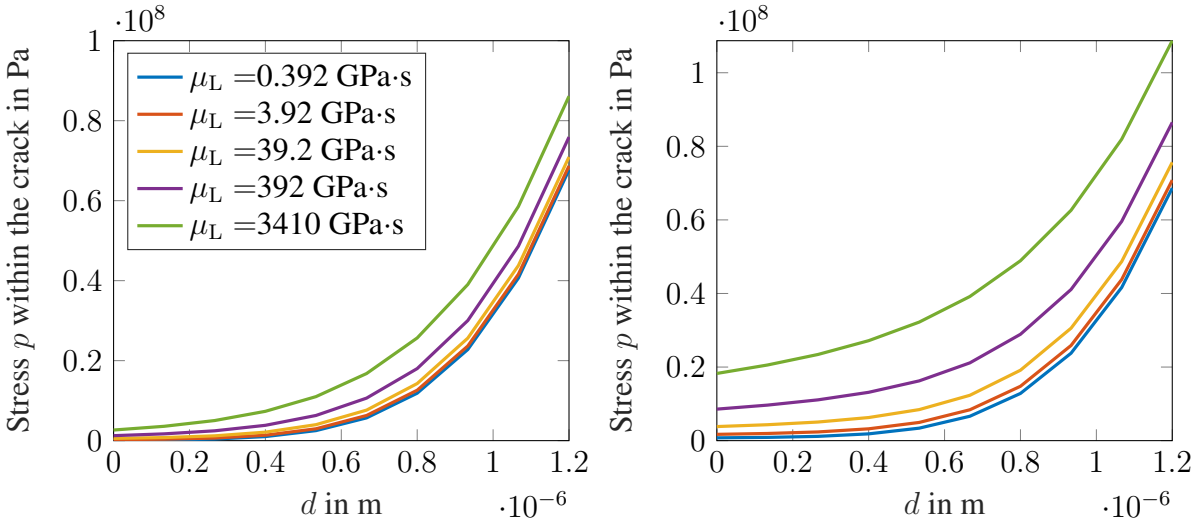

Figure 4.1: Stress inside the crack for $V_{\text{rel}} = 0.01$ (left) and $V_{\text{rel}} = 0.25$ (right)

better representation, the legends in figure 4.2 have been omitted. It should be noted that the legend for the left subplot is the same as in figure 4.1 and on the right side, the lines represent the gel volumes $V_{\text{rel}} = [0.01\ 0.05\ 0.1\ 0.2\ 0.25]$, starting from the blue towards the green line.

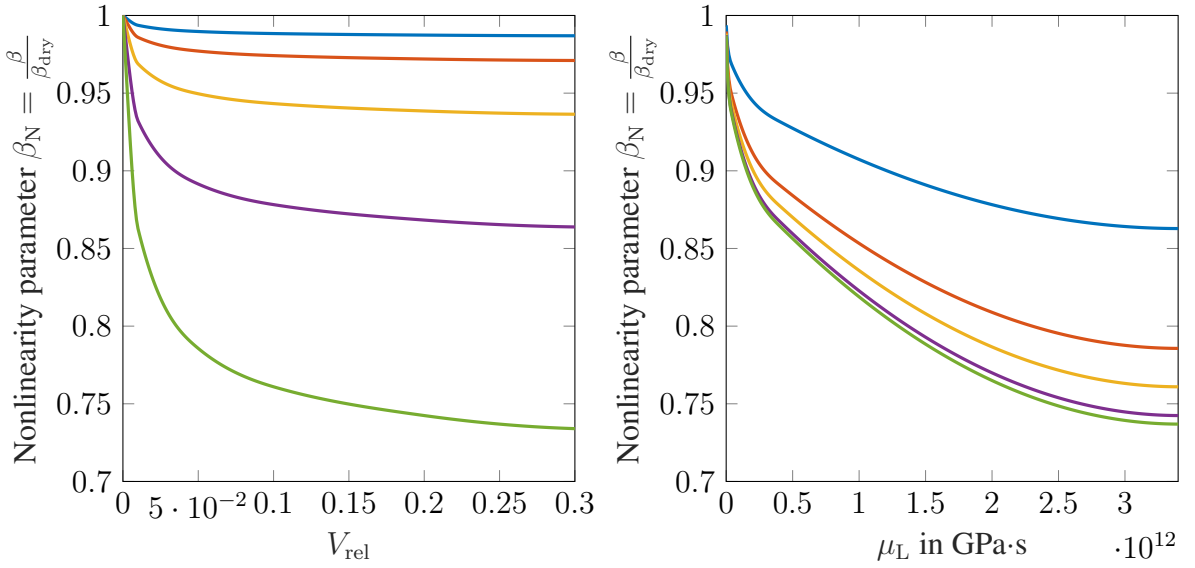

Figure 4.2: β_{N} plotted over the relative volume ratio V_{rel} (left) and over the ASR gel viscosity μ_{L} (right)

According to [34], increasing amounts of (Na + K) dramatically decrease the gel viscosity whereas the calcium content increases it in a nonlinear manner. Therefore, it can be concluded that a detailed research on the gel microstructure is needed to narrow down the range of nonlinearity change.

4.1.2 Asperity height distribution function

The topography of a microcrack can have a significant influence on the overall crack nonlinearity. For instance, if a crack had two flat surfaces, the stiffness of a sample could be described with a Heaviside function which increases the stiffness at the point where the crack is closed. The rougher a surface becomes with time due to various chemical processes, the more does its incremental stiffness depend on the current crack opening and surface morphology. The asperity height distribution further influences the motion of ASR gel during crack closure and therefore, different statistical functions have to be analyzed. These functions, in this work referred to as $\phi(h)$ define the probability of finding asperity peaks at a given location $z = h$. Naturally, many crack surfaces are formed randomly and can be described either by Gaussian or exponential distributions [28, 35] which is in compliance with Longuet-Higgins results for height distribution of moving rough surfaces [36]. A mathematical description of the two functions has been given in equations (3.11) and (3.12) in dependence on σ which is the rms roughness and is studied in the next section.

For the consequent analysis, a rms roughness of $\sigma = 4 \cdot 10^{-7}$ m has been used whereby values differing from the used one up to two orders of magnitude are analyzed in the next section. The remaining parameters for the parametric study are listed in table 4.1.

Figure 4.3 shows the courses of the stress within the crack for dry cracks and the highest considered gel volume. For a brief discussion, three qualitative sections mark the beginning, middle and the final part of flat plane approach. The Gaussian distribution is characterized by a high number of tops around the mean line ($d = 1.2 \cdot 10^{-6}$ m), whereas the exponential one has the highest number of tops in the beginning, i.e. around $d = 0$ m.

Table 4.1: Parameters for calculating the influence of top height distribution function

Parameter	**Value**
Asperity radius	$a = 7 \cdot 10^{-6}$ m
Relative volume ratio	$V_{\text{rel}} = [0; 0.25]$
Mean line location	$m = 1.2 \cdot 10^{-6}$ m
Crack average radius	$R_{\text{avg}} = 10^{-4}$ m
Flat plane approach velocity	$v = 500$ m/s
ASR gel viscosity	$\mu_{\text{L}} = 8.5 \cdot 10^{11}$ Pa·s
El. constants of concrete	$E = 32.517$ GPa and $\nu = 0.231$
Maximum asperity height variation	$R_p = 1.2 \cdot 10^{-6}$ m
rms roughness, standard deviation	$\sigma = 4 \cdot 10^{-7}$ m
Asperity top height distribution	Gaussian, Exponential
Number of cracks per unit volume	$N_0 = 1000$ 1/m^3

For Gaussian, the highest lubrication force values occurs at some distance before the flat plane approach reaches the mean line which appears to be around section 2 of the left subplot. For this reason, the discrepancy between the dry and saturated crack is low around section 1 and then increases towards section 2. Right after section 3, there is still a good amount of tops exerting lubrication force on the flat plane and the discrepancy is almost constant.

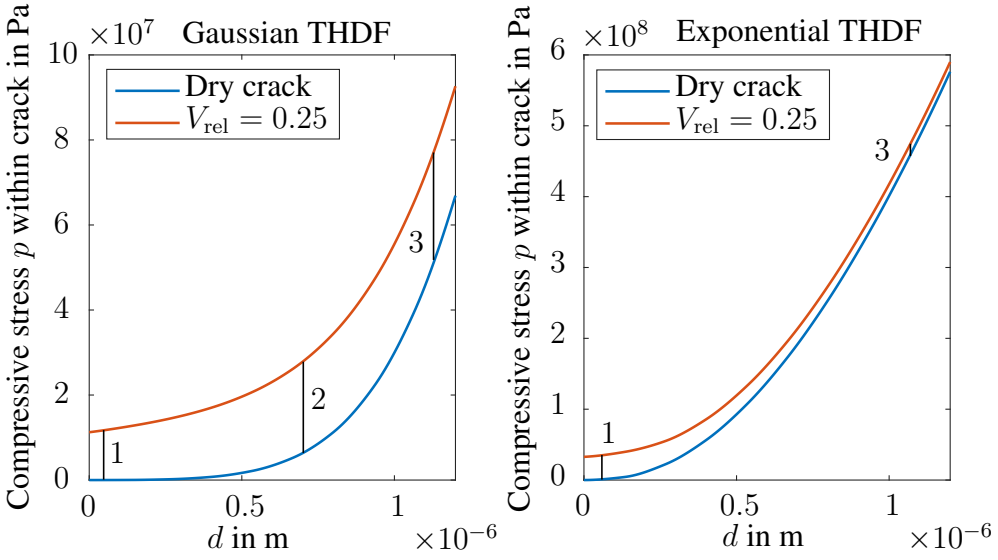

Figure 4.3: Comparison of p for Gaussian and exponential top height distrubutions

For the exponential distribution on the right subplot, the behavior of the curves is different. Around section 1, the number of tops exerting lubrication forces on the flat plane is high and decreases with increasing values for d since the total number of tops decreases. Therefore, the discrepancy between dry and saturated crack falls and the mechanical contact force of the high number of tops located around $d = 0$ rises due to their large deformations. This term occurs in both dry and saturated cracks and the tendency shows that the gel saturated crack approaches the course of the dry crack at higher values for d where the contact force becomes the leading term in the force expressions.

Overall, one recognizes that the normally distributed tops flatten the pressure curve for a filled crack whereas for exponential distribution, the graph is even curved more which indicates than the nonlinearity for exponential distribution may increase due to ASR gel. This tendency is confirmed by plotting the normalized nonlinearity β_{N} and the equilibrium distance d_0 which is illustrated in figure 4.4.

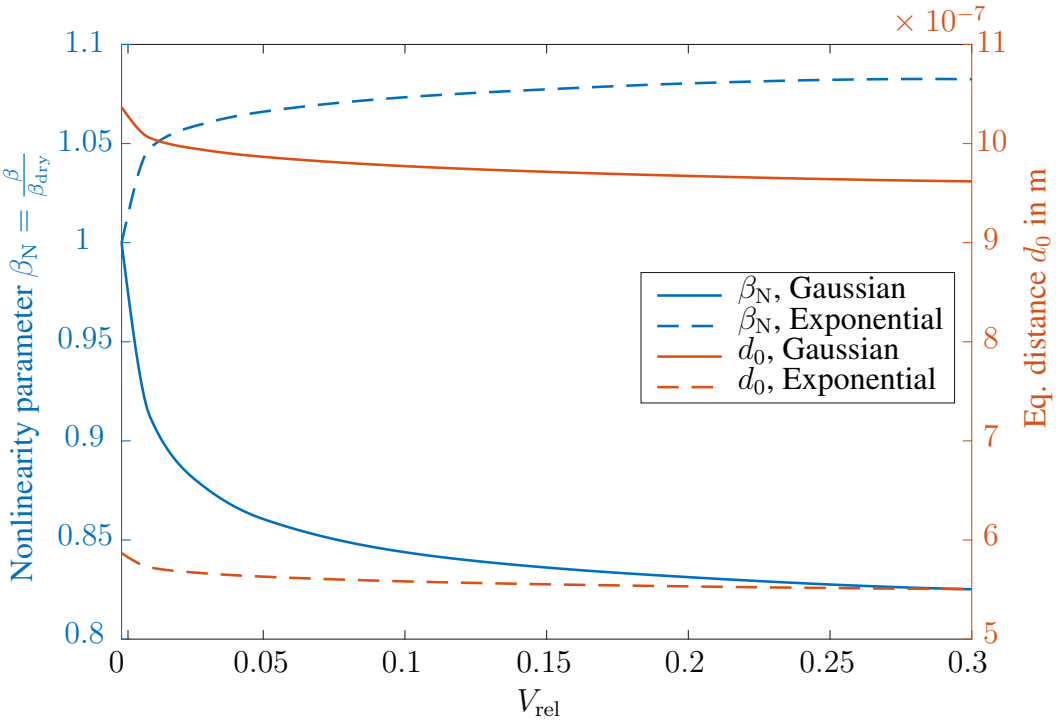

Figure 4.4: Equilibrium distance and normalized nonlinearity for Gaussian and exponential top height distribution

As indicated above, the nonlinearity with Gaussian distribution is reduced to approximately 83% whereas for exponential distribution, it increases by 7%, i.e. the effect of gel is more pronounced for gaussian distribution. Furthermore, the equilibrium distance for exponential distribution is rather independent of the amount of gel when compared to the gaussian one. Also, it is worth noting that the equilibrium opening for exponential distribution is significantly higher since much more asperities are located close to the highest asperity, thus exerting a higher compressive force on the rigid flat plane at larger crack openings (lower values for d).

Summarizing, the nonlinearity change due to ASR gel presence within cracks depends on the distribution of asperity tops. Therefore, an analysis of the processes leading to non-conforming crack surfaces is required in order to obtain an appropriate top height distribution function which enables a more exact calculation of the nonlinearity change.

4.1.3 Root-mean square surface roughness

The effect of surface topography on crack closure properties has been studied by several researchers. An important finding is the intimate relation of closure behavior to crack roughness. Since the stress between two rough surfaces is linked to the normal approach by the interfacial stiffness which again depends on the total number of asperities being in contact at a given approach distance, the standard deviation (rms roughness of composite surface) has a significant influence on the crack nonlinearity. Brown and Scholz [37] have performed experimental measurements with natural rock joints (which behave similarly to cracks in concrete) and figured out that typical surface roughnesses of stone granite and quartzite can vary up to $\sigma = 5 \cdot 10^{-6}$ m. For the parametric studies conducted in this work so far, $\sigma = \frac{1}{3}R_p = 4 \cdot 10^{-7}$ m has been used and is extended to the range proposed by Brown and Scholtz in this section. For consistency reasons, the total number of asperities and thus the gel volume is kept constant which implies that the maximum variation of an asperity height from the mean line, R_p, is adjusted to 3σ in order to keep 99.9% of all

asperities between $h = 0$ and $h = m + R_p$. Since no skewness of the Gaussian distribution is implemented in this work, the distribution remains symmetrical to the mean line and only the height variation increases. The coordinate system origin is always located at the top of the highest asperity, i.e. it is shifted when larger values for σ are considered, thus shifting the coordinate of the mean line in the model (although the mean line does not move in actuality). Figure 4.5 illustrates the courses of the probability density of four different rms roughness values and shows that the crack surface approach for a wider distribution of asperity tops is significantly larger than in the case where all asperities are closer together.

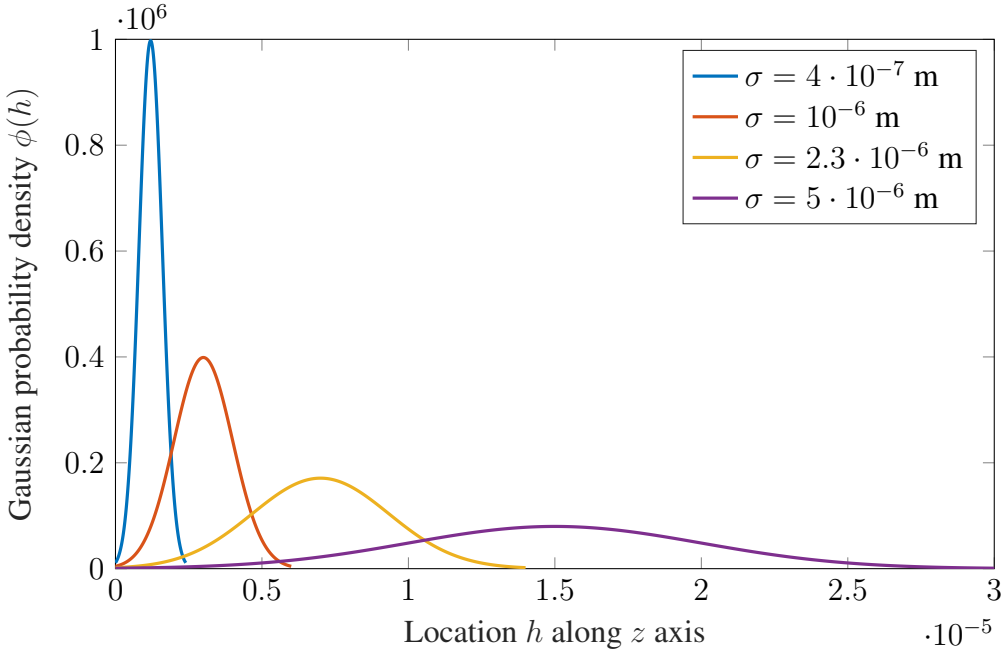

Figure 4.5: Top height distribution for different rms roughness values

To gain a better understanding of the rms roughness effect on the crack nonlinearity, the pressure to flat plane approach relation of dry cracks is investigated next. Therefore, it is appropriate to analyze the stiffness change due to crack closure over a common axis of flat plane approach variation $\tilde{d}$ for several rms roughness parameters where the equilibrium opening of each crack is at $\tilde{d} = 0$.

The cracks of different rms roughness values have identical radii. As long as they are

completely open, the required pressure to further open the crack by the same $\tilde{d}$ is the same since it is dictated by the internal stress in the surrounding solid (figure 4.6). The linear part of the stress $\tilde{p}$ has an offset from graph to graph due to the fact that $\tilde{d}$ has been defined to be 0 at the equilibrium opening d_0 which differs from graph to graph. It is visible that the interfacial stiffness $K = \frac{\partial \tilde{p}}{\partial \tilde{d}}$ is constant and equal for all rms-roughness values as long as the crack surfaces are not yet in contact.

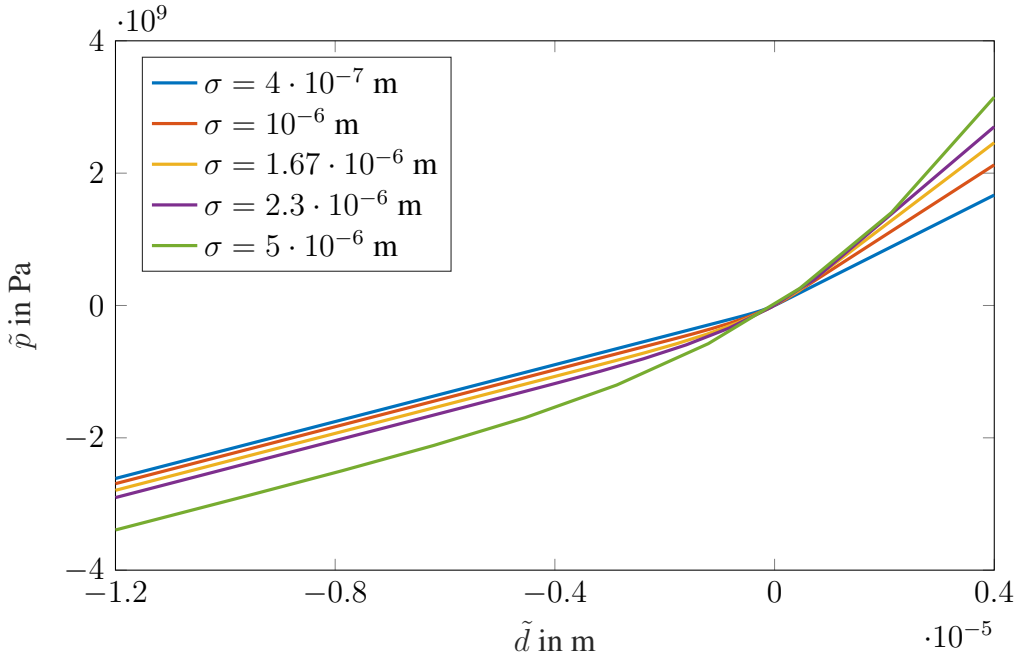

Figure 4.6: Nonlinear stress-approach relationship for various rms roughness values

At some value $\tilde{d}$, the closure process begins and ends when the respective graph becomes linear again. For low rms-roughness values, the distance over which the closure occurs is lower and causes less total deformation of the asperities which increases the stiffness of the solid with a closed crack only a little. On the contrary, a crack of larger rms-roughness (green line) requires a much larger displacement to be closed, thus implying a larger deformation of asperities. It can be recognized that the required stress in order to close the rougher crack is much higher and therefore, it is established that increasing rms-roughness values increase the nonlinear behavior of a cracked medium.

The lubrication force does not depend on the rms-roughness since it no longer exerts pressure on the flat plane once the gel is pushed sideways into a valley between asperities. For this reason, the potential of a given ASR gel volume to reduce nonlinearity stays constant. By implication, this suggests that the relative reduction of nonlinearity has to decrease for increasing σ values which is shown in figure 4.7. The blue line illustrates the rms-roughness already used in figure 4.4 which allows a nonlinearity reduction of 17%. At larger values, it decreases to less than 1% for the implemented configuration (asperity radius, crack radius, gel volumes from table 4.1). An equivalent effect has been observed for exponential top distribution where the initial increase of β_{N} of 7% for $\sigma = 4 \cdot 10^{-7}$ m (figure 4.4) has been found to decrease to less than 1% for $\sigma = 5 \cdot 10^{-6}$ m due to a larger deformation of asperities and thus a lower effect of lubrication.

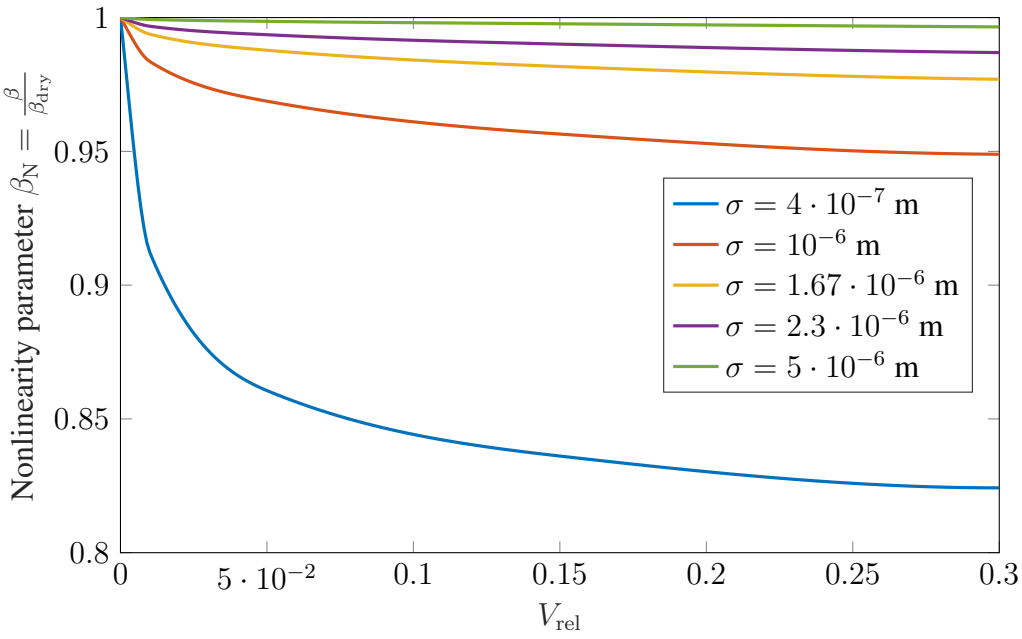

Figure 4.7: Normalized nonlinearity parameter of a cracked medium for different rms-roughness parameters, Gaussian top distribution

Another possible way to investigate this effect would be to calculate the equilibrium crack volume for each rms-roughness value and then prescribe a respective gel volume such that the ratio of crack volume to gel volume is kept constant. This would require

an adjustment of either the asperity radius or number of asperities in order to keep the negligence of "gel blocks" interaction with each other valid. One would need to analyze the maximum wetting of each asperity during the flat plane approach and make sure it does not exceed the asperity radius. In case it does, lateral spacing between asperities has to be increased or the effect of gel blocks pushing laterally against one another has to be accounted for.

To summarize, the roughness of crack surfaces has a significant impact on the nonlinearity reduction caused by ASR gel. The main reason herefore is the larger deformation a rougher crack experiences wherefore the mechanical contact force rises in magnitude when compared to the lubrication force. Therefore, a detailed measurement and analysis of the crack topography is inevitable in order to obtain accurate results for the nonlinearity parameter β_{N}.

4.2 Simulation with distributed crack sizes and varying crack density

In section 3.7, the nonlinearity parameter of a cracked medium has been derived using an averaged crack radius R_{avg} for simplicity whereby a closed form expression for C_{N} has been obtained. It should be noted that in a real application, the crack size is a function of time with changing limits. Shortly after the gel pressure at the interface between an aggregate and the surrounding matrix has exceeded the tensile limit of the matrix, a certain number of microcracks with small sizes are formed. As time goes by and more gel is produced, the cracks grow in size and new ones are generated simultaneously wherefore the crack density increases too. Then, the crack size distribution can be described by a distribution function (similar to the top height distribution) which is assumed to be Gaussian at first. The maximum crack radius at a given time is denoted by R_{max} and the distribution is characterized by its standard deviation σ_{R} in addition. Performing accurate experiments on crack sizes within a volume is an involved task since a specimen would need to be cut in order to measure the crack sizes in its interior which again can produce further cracks and

thus complicate the distinction between originally present cracks and new ones induced by the cutting process. Therefore, it can be accepted that a regular standard deviation of $\sigma_{\mathrm{R}} = \frac{1}{6} R_{\max}$ holds for all distributions and the crack sizes are always distributed with the given standard deviation between 0 and $R_{\max}$. Following these approximations, the linear and nonlinear compliances are written as

$$\begin{aligned} S_{\mathrm{L}} &= \frac{1}{E} + N_0 \, cos^4\left(\theta_{\mathrm{avg}}\right) \pi \int_0^{R_{\max}} \alpha_{\mathrm{cr}}(R) \, \phi_{\mathrm{R}}\left(R, R_{\max}\right) R^2 dR \\ S_{\mathrm{N}} &= \frac{N_0}{2} \, cos^6\left(\theta_{\mathrm{avg}}\right) \pi \int_0^{R_{\max}} \beta_{\mathrm{cr}}(R) \, \phi_{\mathrm{R}}\left(R, R_{\max}\right) R^2 dR \end{aligned} \tag{4.4}$$

where the Gaussian distribution is given by

$$\phi_{\mathrm{R}}\left(R, R_{\max}\right) = \frac{6}{\sqrt{2\pi} R_{\max}} \exp\left(-\frac{36}{2 R_{\max}^2} (R - 0.5 R_{\max})^2 \right) \tag{4.5}$$

The linear and nonlinear elastic constants are obtained from a series reversion and yield

$$\begin{aligned} C_{\mathrm{L}} = \frac{1}{S_{\mathrm{L}}} &= \frac{E}{1 + E N_0 \, cos^4\left(\theta_{\mathrm{avg}}\right) \pi \int_0^{R_{\max}} \alpha_{\mathrm{cr}}(R) \, \phi_{\mathrm{R}}\left(R, R_{\max}\right) R^2 dR} \\ C_{\mathrm{N}} = -\frac{S_{\mathrm{N}}}{S_{\mathrm{L}}^3} &= \frac{\frac{N_0}{2} cos^6\left(\theta_{\mathrm{avg}}\right) \pi \int_0^{R_{\max}} \beta_{\mathrm{cr}}(R) \, \phi_{\mathrm{R}}\left(R, R_{\max}\right) R^2 dR}{\left(\frac{1}{E} + N_0 \, cos^4\left(\theta_{\mathrm{avg}}\right) \pi \int_0^{R_{\max}} \alpha_{\mathrm{cr}}(R) \, \phi_{\mathrm{R}}\left(R, R_{\max}\right) R^2 dR \right)^3} \end{aligned} \tag{4.6}$$

Recalling that α_{cr} and β_{cr} are linear and nonlinear coefficients of a single crack (should not be interchanged with the linear and nonlinear elastic constants of a medium) which have been obtained numerically due to the complexity of the force expression, one recognizes that they can not be given as a closed form term of the crack radius in order to integrate with respect to R. For this reason, the integrals in equation (4.6) are computed using a Gauss-Legendre quadrature of the following relation

$$\int_a^b f(x) dx = \frac{b-a}{2} \sum_{i=1}^{n} f\left(\frac{b-a}{2} x_i + \frac{a+b}{2} \right) \omega_i \tag{4.7}$$

where x_i and ω_i are called nodes and weights, respectively, at specific points which depend on the number of points used n. The right side of equation (4.7) scales the nodes and weights to the integration limits $a = 0$ and $b = R_{\max}$. Exemplary, a division into ten sections, $n = 9$, yields the nodes and weights shown in table 4.2.

Table 4.2: Gauss quadrature: nodes and weights for $n = 9$

i	**Node** x_i	**Weight** ω_i	i	**Node** x_i	**Weight** ω_i
1	-0.9682	0.0813	6	0.3243	0.3123
2	-0.836	0.1806	7	0.6134	0.2606
3	-0.6134	0.2606	8	0.836	0.1806
4	-0.3243	0.3123	9	0.9682	0.0813
5	0	0.3302			

Subsequently, the integrals in equation (4.6) need to be evaluated at the transformed nodes given in equation (4.7). Starting with small crack sizes, the range is varied along with the crack density in order to yield results for different crack images which can develop over time. The integrals in equation (4.6) are written as

$$\begin{aligned}
\int_0^{R_{\max}} \alpha_{\mathrm{cr}}(R)\ \phi_{\mathrm{R}}\left(R, R_{\max}\right) R^2 dR &= \frac{R_{\max}}{2} \sum_{i=1}^{n} \alpha_{\mathrm{cr}} \left(\frac{R_{\max}}{2} x_i + \frac{R_{\max}}{2} \right) \\
&\quad \phi_{\mathrm{R}} \left(\frac{R_{\max}}{2} x_i + \frac{R_{\max}}{2} \right) \left(\frac{R_{\max}}{2} x_i + \frac{R_{\max}}{2} \right)^2 \omega_i \\
\int_0^{R_{\max}} \beta_{\mathrm{cr}}(R)\ \phi_{\mathrm{R}}\left(R, R_{\max}\right) R^2 dR &= \frac{R_{\max}}{2} \sum_{i=1}^{n} \beta_{\mathrm{cr}} \left(\frac{R_{\max}}{2} x_i + \frac{R_{\max}}{2} \right) \\
&\quad \phi_{\mathrm{R}} \left(\frac{R_{\max}}{2} x_i + \frac{R_{\max}}{2} \right) \left(\frac{R_{\max}}{2} x_i + \frac{R_{\max}}{2} \right)^2 \omega_i
\end{aligned} \tag{4.8}$$

Using these expressions, the linear and nonlinear constants are calculated again and plotted for varying maximum crack radii, $R_{\max}$, in figure 4.8 whereby the crack density has been kept constant at $N = 1000\ \mathrm{m}^{-3}$. For comparison purposes, additional graphs have been generated with averaged crack sizes whereby $R_{\mathrm{avg}} = R_{\mathrm{mean}} = R_{\max}/2$. For the given

configuration, increased $R_{\max}$ implies an increasing total volume of cracks and thus an increasing total nonlinearity. Since the gel volume to asperity volume ratio V_{rel} is a prescribed value, increasing crack radius (and thus increasing number of asperities per crack) means that the total gel volume is increased as well which in fact, is one of the main reason for microcrack growth. Therefore, there is a larger potential of nonlinearity reduction with increasing crack sizes.

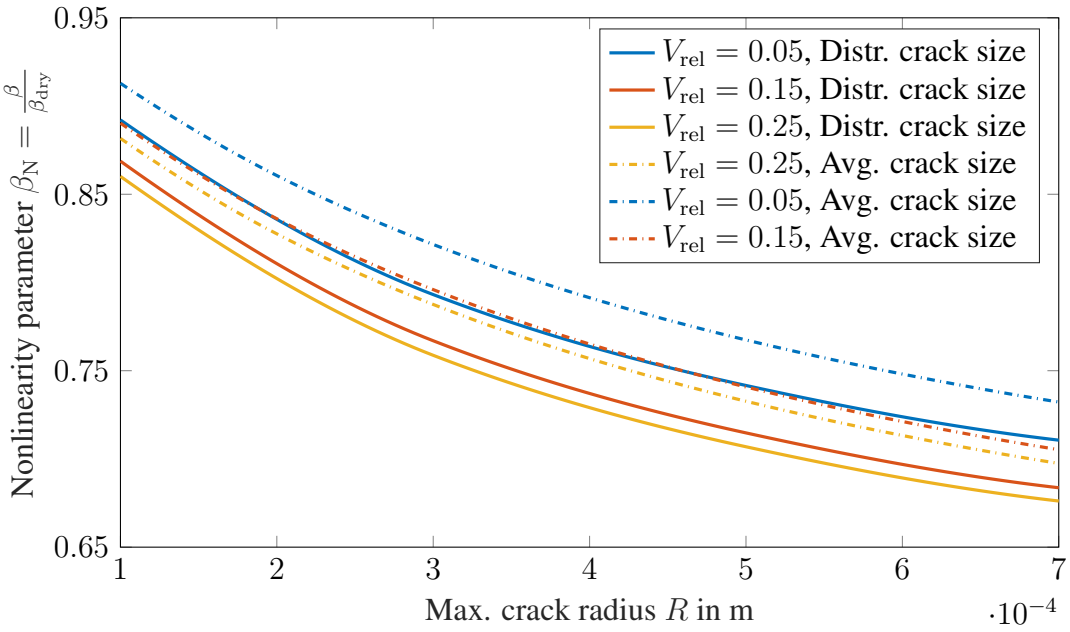

Figure 4.8: Normalized nonlinearity parameter of a cracked medium for different crack radii

One recognizes that the nonlinearity can be reduced by 14% for a maximum crack size of 0.1 mm whereas there is a significantly higher reduction if the maximum crack radius is increased to 0.7 mm. Also, approximating the crack radius distribution by an averaged radius appears to underestimate the nonlinearity reduction by roughly 3% wherefore an implementation of the more accurate normal distribution is recommended. Unfortunately, performing experimental studies on microcracks is a difficult task and the accurate choice of suitable crack sizes is therefore limited. It becomes even more involved when the influence of ASR gel is to be accounted for since the exact motion of ASR gel along crack

surfaces has not been investigated sufficiently yet. However, the model in hand allows some estimations towards the dependence of the nonlinearity on the most important parameters.

Furthermore, it has been found that the crack density N does not really affect the normalized nonlinearity β_{N} for given gel volumes, although the total nonlinearity β is a function of N. Hence, increasing N from 10^3 to 10^4 and then to 10^5 m^{-3} changed the normalized nonlinearity by less than a third percent. It can be concluded that the nonlinearity reduction due to ASR gel depends stronger on the topography and size of a single crack than on the total number of cracks per unit volume of a cracked medium.

For all simulation results so far, the nonlinearity reduction due to ASR gel has been given as a normalized value by the nonlinearity of a dry crack. However, an interesting aspect is given in the analysis of the total nonlinearity of a medium and how it is affected by the crack size or density. In fact, a significant change has been observed when varying one of these parameters. This observation is clarified in figure 4.9.

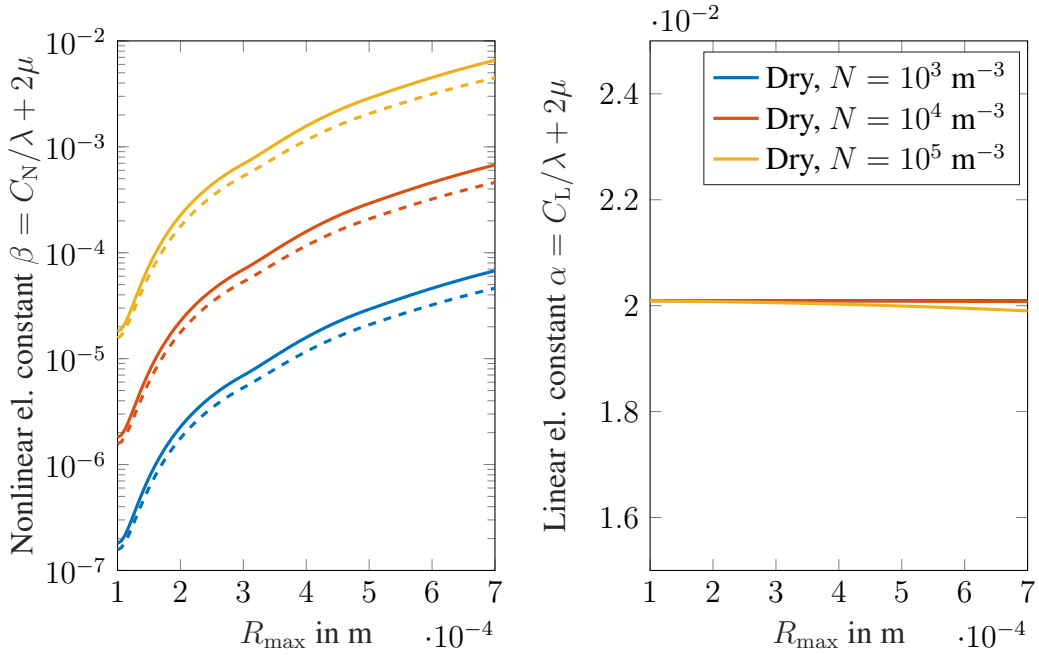

Figure 4.9: Dependency of linear and nonlinear elastic constants on maximum crack radius and crack density

The solid lines represent the values for a dry crack whereas the dashed lines illustrate

a relative ASR gel volume of $V_{\mathrm{rel}} = 0.15$. On the right subplot, the partially filled cracks have been omitted due to the negligible influence of gel on the linear elastic constant.

Figure 4.9 can be looked at from two points of view. First, it is realized that at a fixed maximum crack radius (x- axis), the nonlinear constant of elasticity increases by several orders of magnitude when the crack density is increased. Second, at a fixed crack density, increasing the crack radius rises the nonlinear constant up to two orders of magnitude as well. It can be concluded that the nonlinear constant is very sensitive to both crack size and crack density. On the contrary, the linear constant of elasticity (right subplot) shows almost no sensitivity to neither crack size or crack density. For this reason, nonlinear techniques are inevitable towards the determination and analysis of microcracks as these include the nonlinear behavior of microcracks. Linear techniques by contrast only include the linear material parameters which change so little that no appropriate statement can be made about either size and density of microcracks or the influence of ASR gel on the crack behavior.

4.3 Estimation of nonlinearity development over time

In this section, some estimations towards the development of a cracked solid's nonlinearity over time are performed. The objective of the section is to simulate the change of acoustic nonlinearity during the process of ASR where gel formation and consequent microcrack growth are all involved in a function of time. The main parameters which are altered with time are the crack density N, the maximum crack radius $R_{\max}$ and the gel amount per pair of asperities, denoted by V_{rel}. The exact determination of their dependency on time involves solving diffusion laws including water imbibition and alkali ion diffusion or physical transport laws which describe how fast the gel flows into the cracks. For this reason, reasonable approximations about these three parameters are made in order to show the qualitative development of the nonlinearity over time. A common trend in the nonlinearity evolution observed from multiple experiments on concrete and mortar specimens [1] with reactive aggregates is a rapid increase until saturation and then decrease with time. It is therefore of

major importance to examine if the model developed in this thesis is capable of predicting such a common behavior.

A logical course of the parameter's growth is given by splitting the crack formation and the crack saturation process into two main regimes. It is assumed that during the first 100 days of a total analysis time of one year, gel is mainly formed at the ITZs and causes a rapid formation of a number of "dry" microcracks. These can be either numerous and small in size or large but therefore less in quantity, depending on the medium inhomogeneity.

Hence, the crack density N is the main parameter which grows during the first regime whereas the maximum crack radius is constantly low and no gel is present within the cracks. In the second regime which ranges from day 100 up to 365, the gel starts to flow into the microcracks and causes their continuos saturation such that V_{rel} increases since more gel is formed and flows into the cracks. On the contrary, the crack density no longer increases due to the released gel pressure at the interface between aggregates and the cement paste.

Table 4.3: Parameter development for different configurations over time

t [d]	$R_{\mathrm{max},1}$ [m]	N_1 [m^{-3}]	$V_{\mathrm{rel},1}$	$R_{\mathrm{max},2}$	N_2	$V_{\mathrm{rel},2}$	$R_{\mathrm{max},3}$	N_3	$V_{\mathrm{rel},3}$
0	0	0	0	0	0	0	0	0	0
50	$1.05 \cdot 10^{-4}$	450	0	$1.2 \cdot 10^{-4}$	400	0	$5 \cdot 10^{-4}$	12	0
100	$1.05 \cdot 10^{-4}$	1000	0	$1.2 \cdot 10^{-4}$	1200	0	$5 \cdot 10^{-4}$	20	0
150	$1.05 \cdot 10^{-4}$	1020	0.1	$1.2 \cdot 10^{-4}$	1200	0	$5 \cdot 10^{-4}$	20	0.005
200	$1.05 \cdot 10^{-4}$	1020	0.15	$1.2 \cdot 10^{-4}$	1200	0.02	$5 \cdot 10^{-4}$	20	0.01
250	$1.05 \cdot 10^{-4}$	1020	0.2	$1.2 \cdot 10^{-4}$	1200	0.05	$5 \cdot 10^{-4}$	20	0.01
300	$1.05 \cdot 10^{-4}$	1020	0.2	$1.2 \cdot 10^{-4}$	1200	0.08	$5 \cdot 10^{-4}$	20	0.015
350	$1.05 \cdot 10^{-4}$	1020	0.25	$1.2 \cdot 10^{-4}$	1200	0.1	$5 \cdot 10^{-4}$	20	0.02

Table 4.3 shows three possible configurations of the main parameters, classified by a subscript $1(1)3$. The first two configurations are characterized by lower crack sizes at higher crack densities whereas the third one contains a lower number of larger cracks. Due to the fact that the gel volume per asperity is linked to the asperity volume which has been kept constant, increasing the crack radius means that the number of asperities per crack and

thus the total gel volume in the crack increases as well.

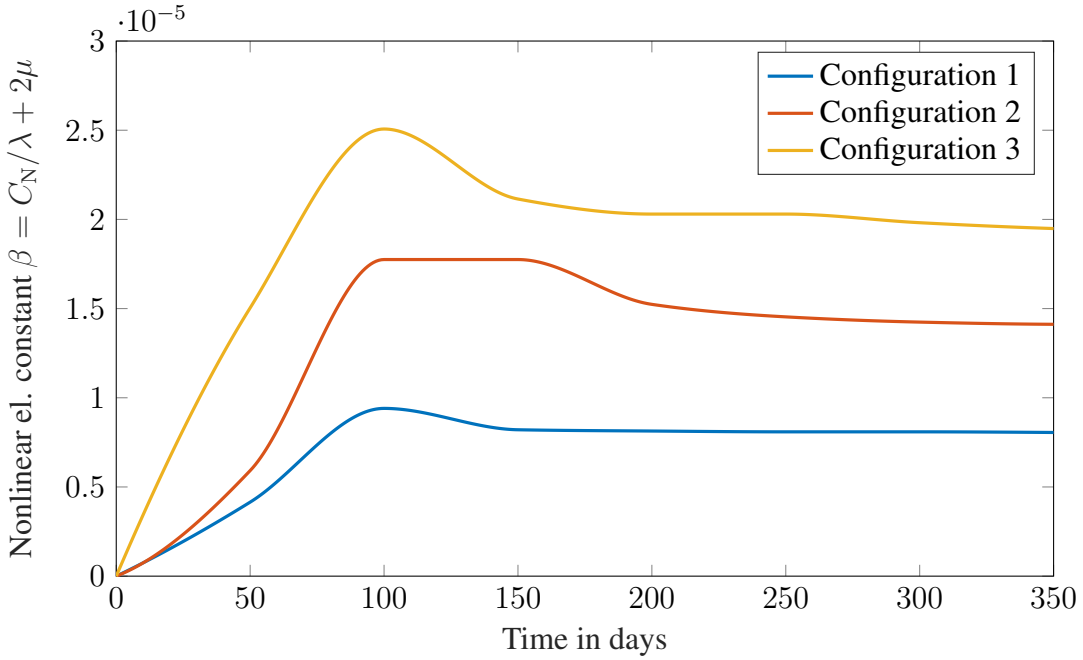

Figure 4.10: Exemplary development of nonlinearity parameter β [-] over time

In consequence, V_{rel} has been lowered at higher crack radii in order to avoid full crack saturation with gel (which would require that gel block interaction with other blocks is accounted for). The remaining simulation parameters have been assumed to be those from table 4.1. The trends of the two regimes seem clear in figure 4.10. The generation of dry cracks in the first 100 days causes the nonlinearity to increase (as already indicated in figure 4.9), followed by a reduction once the crack surfaces are lubricated with gel. Depending on how exactly the crack density and crack size develop against the amount of gel within the cracks, it can happen that the nonlinearity decreases, stays constant or even increases further. However, once enough gel is produced and pushed into the cracks, the pressure at the ITZ decreases significantly such that the number of cracks stays constant. Since the microcracks would not increase in size until they are completely filled with gel, the process of crack saturation with gel is likely to decrease the nonlinearity of a cracked medium which is in compliance with performed measurements.

CHAPTER 5
SUMMARY AND OUTLOOK

5.1 Summary

In the present work, the reduction of a solid's nonlinear behavior due to the presence of ASR gel between crack surfaces has been analyzed. For this purpose, a nonlinear stress to crack closure relation has been developed, employing the lubrication force of the gel in addition to the Hertzian force which characterizes the mechanical contact of crack asperities. The nonlinear tensile stress between crack surfaces has been superimposed with the oppositely directed stress in the surrounding solid which acts against the crack opening and resists compressive deformations. The crack opening at which both components are equal in magnitude has been denoted as the equilibrium crack opening displacement. Since a small approach variation from the equilibrium opening requires an additional stress which equals to the difference of the stress component within the crack and the internal stress in the solid around the crack, a nonlinear equation up to the second order has been fit to the numerically obtained expression for the caused stress difference. Due to the complexity of the lubrication force term, an analytical solution can not be provided so that numerical calculation is necessary. It has been found that already small amounts of ASR gel indeed reduce the nonlinearity of a crack closure since compressive lubrication forces occur before a mechanical contact and thereby straighten the pressure course. This effect is enhanced by increasing the amount of gel such that a tendency of decreased nonlinearity with increased gel amounts has been observed. Further, it is pointed out that the equilibrium opening of a crack increases with increasing amounts of ASR gel which is one of the reasons why concrete samples expand in size over time.

A parametric study on the gel composition has indicated that gels of higher viscosities

are capable of reducing the nonlinearity in a stronger manner by providing higher resistance against crack closure. Also, the height distribution of tops within a crack significantly affects the nonlinearity change. For a Gaussian distribution where the largest number of tops is located around the middle line, large resistance due to ASR gel flow is exerted on the approaching flat plane when the crack is half closed. This actually straightens the pressure curve and leads to a decrease in nonlinearity. On the contrary, an exponential distribution which is characterized by a large number of asperities at high locations indicates that the largest resistance due to ASR gel occurs in the beginning of the approach, i.e. when the crack is fully opened. This results in an additional curving of the already nonlinear pressure course and thus an increased nonlinearity.

The root mean square roughness of a crack has been shown to influence the nonlinearity change as well. Cracks characterized by rougher surfaces exhibit a more pronounced nonlinear behavior due to larger deformations during crack closure and thus a larger change in stiffness between a fully opened and fully closed crack. Since the magnitude of the lubrication force does not change with increased rms-roughness, the effect of ASR gel decays for rougher cracks. This is caused by the increased magnitude of Hertzian contact force wherefore the mechanical contact becomes more leading in the overall force expression term. Hence, the nonlinearity reduction for Gaussian distribution and the nonlinearity increase for exponential distribution are both decreased at higher rms-roughness values.

In section 4.2, the distributed size of microcracks has been investigated with the result of a more reduced nonlinearity for larger crack sizes. This finding can be explained by the fact that a prescribed gel volume to asperity volume ratio means higher amounts of ASR gel for larger cracks due to the fact that the number of asperities increases during crack growth. Furthermore, approximating the crack size distribution by an averaged crack size is shown to underestimate the nonlinearity change by ca. 3%. Since the computational effort is not significantly higher for distributed crack sizes, it is recommended to account for this aspect which represents the real appearance of microcracks more accurately. Also,

it has been found that the normalized nonlinearity β_{N} rather depends on the distribution of cracks sizes and their topography than on the crack density although the total nonlinearity β is an almost linear function of the crack density N.

Lastly, section 4.3 shows a conceivable course of the nonlinearity over time with suitably selected parameters. The developed model is shown to be capable of reproducing the initially increasing and then decreasing nonlinearity behavior observed in experimental studies.

5.2 Outlook and future work

It should be noted that the stress in the surrounding solid has been approximated by a linear function which is subject to the assumption of a linear elastic behavior of the concrete without cracks. Although this is a widely used assumption, in actuality, even a crack free concrete does not behave linearly. In case this aspect needed to be included into the analysis, a more complex non-linear stress-displacement relationship would be required in order to describe the stress in the surrounding solid. Conceivably, the nonlinearity reduction would be altered by this adjustment since the overall total nonlinearity would no longer originate from microcracks only and one would need to investigate the weighting of nonlinearity due to cracks and due to intact solid. However, nonlinearity due to microcracks is typically more pronounced than the nonlinear behavior of intact solid such that a reduction due to ASR gel within a crack would be still achieved.

The second aspect that could be approached from a different point of view is the distribution of gel. In this work, the method used to model the gel is dictated by the derivation of a lubrication force. Since the lubrication force between two spherical asperities has been found to be an integral of a pressure distribution over the area which is covered in gel, a suitable model of the liquid is achieved by distributing the total amount of gel over all asperities. Hence, each asperity is covered in gel up to a certain lateral coordinate from its middle line which is derived from the prescribed gel amount and the distance between

asperities. Then, the extent to which an asperity is covered in gel increases as the flat plane gets closer to an asperity and the lubrication force rises. Each pair of asperities confines a ”block” of gel which conserves its volume throughout the relative approach of the surfaces and acts independently of neighboring pairs of asperities. Another, possibly more accurate yet way more involved approach to model the gel is to distribute a given gel volume in such a way that the valleys between asperities are filled first and the gel has a constant height throughout the crack. Then, increasing the gel amount would result in an increased height of the gel layer. As indicated, there is no way to simplify such a model to a single pair of asperities for which a force expression can be obtained and then integrated over all asperities to calculate the entire crack's nonlinearity. As a consequence, a hydrodynamical model would need to be developed which is capable of solving the partial differential equations for the fluid motion and its resistance against crack closure. Simultaneously, effects such as crack growth could be investigated in a detailed manner which in turn, is an advantageous point of a more complex computational model as it would be able to capture the time-dependent change of crack sizes (section 4.2) accurately. Moreover, assumptions such as the steady motion of the crack surfaces would not need to be made since decelerating effects due to the ASR resistance would be included in the calculation automatically.

Based on the modeling approach for the ASR gel, asperities of opposing crack surfaces have been assumed to be located along a common axis of rotational symmetry, i.e. the mechanical contact can be described by the Hertzian theory of contacting spheres (or a sphere being brought into contact with an elastic half-space). In a future work, the model could be extended to the case where the asperities are laterally shifted relative to each other such that the occurring force is not only normal to the crack surface but also contains a component which causes sliding/transverse forces along the crack surface. In such a configuration, an additional degree of freedom of the asperities has to be accounted for which could possibly result in a reduced crack nonlinearity since the lateral sliding would lead to a decrease of the normal stress.

In section 4.1.1, it has been shown that a proper and detailed knowledge of the ASR gel viscosity is crucial towards a narrowed range of possible results. Due to the lack of extensive measurements, only the results from [34] have been used in this work. However, the paper shows a wide range of gel viscosities that can be common for ASR gel based on its diverse chemical composition. Furthermore, the paper uses only stress-strain results over time and fits these into a Burger's model. In order to obtain narrowed ranges for a certain application, it would be helpful to create gel specimens from known chemical compositions and measure their viscosity using accurate methods such as capillary, vibrational or rotational viscometers. Knowing the amounts of all chemical parts within a concrete specimen would then allow a precise calculation and validation of the proposed nonlinearity change.

Moreover, proper investigation of the crack topography development over time is needed to quantify the nonlinearity change in greater detail. In section 4.1.1, the surface topography has been shown to have a notable impact on the nonlinearity. In actuality, the distribution of asperity heights as well as their rms-roughness can alter as a result of various chemical or mechanical processes which occur in different degrees over time. Hence, a detailed model for surface roughening/softening would allow a time-dependent representation of the crack surface parameters and consequently a more appropriate description of the nonlinearity with respect to time.

In section 4.3, a qualitative analysis of the nonlinearity parameter's history has been performed whereby reasonable assumptions for crack growth, multiplication and ASR gel flux into the microcracks have been made. In order to further improve this section, physical transport and diffusivity laws could be implemented to describe the gel production process and thus the crack growth over time. Such an extension would allow an exact calculation not only of the pressure at the ITZ which leads to cracking but also the gel amount present within the cracks at every time step. Further, this would yield the possibility to accurately predict when a crack is fully saturated with gel and consequently its growth rate.

Summarizing, the model in hand allows predictions towards the nonlinear behavior of

a cracked medium in which ASR gel is produced. By substituting respective material constants, the nonlinearity of several kinds of materials subjected to Alkali-silica reaction such as mortar and concrete can be quantified. Due to the diversity of several model parameters, experimental measurements with specimens of known compositions are recommended for the purpose of model validation. Further model extensions are possible in order to improve the model depth, specifically with respect to time.

REFERENCES

[1] K. J. Leśnicki, J.-Y. Kim, K. E. Kurtis, and L. J. Jacobs, "Assessment of alkali–silica reaction damage through quantification of concrete nonlinearity," *Materials and structures*, vol. 46, no. 3, pp. 497–509, 2013.

[2] R. D. Mindlin, "Compliance of elastic bodies in contact," *J. Appl. Mech., ASME*, vol. 16, pp. 259–268, 1949.

[3] K. L. Johnson and K. L. Johnson, *Contact mechanics*. Cambridge university press, 1987.

[4] I. Sevostianov and M. Kachanov, "Contact of rough surfaces: A simple model for elasticity, conductivity and cross-property connections," *Journal of the Mechanics and Physics of Solids*, vol. 56, no. 4, pp. 1380–1400, 2008.

[5] J. A. Greenwood and J. P. Williamson, "Contact of nominally flat surfaces," *Proceedings of the royal society of London. Series A. Mathematical and physical sciences*, vol. 295, no. 1442, pp. 300–319, 1966.

[6] V. E. Nazarov and A. M. Sutin, "Nonlinear elastic constants of solids with cracks," *The Journal of the Acoustical Society of America*, vol. 102, no. 6, pp. 3349–3354, 1997.

[7] V. Nazarov, "Acoustic nonlinearity of cracks partially filled with liquid: Cubic approximation," *The Journal of the Acoustical Society of America*, vol. 109, no. 6, pp. 2642–2648, 2001.

[8] H. Brenner, "The slow motion of a sphere through a viscous fluid towards a plane surface," *Chemical engineering science*, vol. 16, no. 3-4, pp. 242–251, 1961.

[9] B. Lambert, L. Weynans, and M. Bergmann, "Local lubrication model for spherical particles within incompressible navier-stokes flows," *Physical Review E*, vol. 97, no. 3, p. 033 313, 2018.

[10] O. I. Vinogradova, "Drainage of a thin liquid film confined between hydrophobic surfaces," *Langmuir*, vol. 11, no. 6, pp. 2213–2220, 1995.

[11] A Vázquez-Quesada and M Ellero, "Analytical solution for the lubrication force between two spheres in a bi-viscous fluid," *Physics of Fluids*, vol. 28, no. 7, p. 073 101, 2016.

[12] M. E. Gurtin, E. Fried, and L. Anand, *The mechanics and thermodynamics of continua*. Cambridge University Press, 2010.

[13] M. E. Gurtin, *An introduction to continuum mechanics*. Academic press, 1982.

[14] S. Eldevik, "Measurement of non-linear acoustoelastic effect in steel using acoustic resonance," 2014.

[15] R. W. Ogden, *Non-linear elastic deformations*. Courier Corporation, 1997.

[16] F. D. Murnaghan, *Finite deformation of an elastic solid*. Wiley, 1951.

[17] H Hertz, *Über die berührung fester elastischer körper: Gesammelte werke*, 1895.

[18] C. Navier, "Mémoire sur les lois du mouvement des fluides," *Mémoires de lAcadémie Royale des Sciences de lInstitut de France*, vol. 6, no. 1823, pp. 389–440, 1823.

[19] H. Brenner, "The slow motion of a sphere through a viscous fluid towards a plane surface," *Chemical engineering science*, vol. 16, no. 3-4, pp. 242–251, 1961.

[20] D. Y. Chan and R. Horn, "The drainage of thin liquid films between solid surfaces," *The Journal of chemical physics*, vol. 83, no. 10, pp. 5311–5324, 1985.

[21] J.-J. Shu, J. Bin Melvin Teo, and W. Kong Chan, "Fluid velocity slip and temperature jump at a solid surface," *Applied Mechanics Reviews*, vol. 69, no. 2, 2017.

[22] B. J. Hamrock, S. R. Schmid, and B. O. Jacobson, *Fundamentals of fluid film lubrication*. CRC press, 2004, pp. 181–190.

[23] I. N. Sneddon, "The distribution of stress in the neighbourhood of a crack in an elastic solid," *Proceedings of the Royal Society of London. Series A. Mathematical and Physical Sciences*, vol. 187, no. 1009, pp. 229–260, 1946.

[24] P Cornetti and A Sapora, "Penny-shaped cracks by finite fracture mechanics," *International Journal of Fracture*, vol. 219, no. 1, pp. 153–159, 2019.

[25] J. R. Barber, *Elasticity*. Springer, 1992.

[26] S. Multon, A. Sellier, and M. Cyr, "Chemo–mechanical modeling for prediction of alkali silica reaction (asr) expansion," *Cement and Concrete Research*, vol. 39, no. 6, pp. 490–500, 2009.

[27] B Chiaia, "Experimental determination of the fractal dimension of microcrack patterns and fracture surfaces," in *Fractals and Fractional Calculus in Continuum Mechanics*, Springer, 1997, pp. 57–107.

[28] B. Bhushan, "Surface roughness analysis and measurement techniques," in *Modern Tribology Handbook, Two Volume Set*, CRC press, 2000, pp. 79–150.

[29] T. R. Thomas and T. R. Thomas, *Rough surfaces*. World Scientific, 1999, vol. 278.

[30] T. Wu, *A Multiscale/multiphysics Model for Concrete*. Inst. für Kontinuumsmechanik, Gottfried-Wilhelm-Leibniz-Univ., 2014.

[31] R. E. Jones, "Models for contact loading and unloading of a rough surface," *International Journal of Engineering Science*, vol. 42, no. 17-18, pp. 1931–1947, 2004.

[32] N. Yoshioka, "A review of the micromechanical approach to the physics of contacting surfaces," *Tectonophysics*, vol. 277, no. 1-3, pp. 29–40, 1997.

[33] C. Pecorari, "Modeling non-collinear mixing by distributions of clapping microcracks," *Wave Motion*, vol. 59, pp. 69–80, 2015.

[34] A. Gholizadeh-Vayghan, F. Rajabipour, M. Khaghani, and M. Hillman, "Characterization of viscoelastic behavior of synthetic alkali–silica reaction gels," *Cement and Concrete Composites*, vol. 104, p. 103 359, 2019.

[35] A Baltazar, J. Kim, and S. Rokhlin, "Ultrasonic determination of real contact area of randomly rough surfaces in elastoplastic contact," *Revista mexicana de física*, vol. 52, no. 1, pp. 37–47, 2006.

[36] M. S. Longuet-Higgins, "The statistical analysis of a random, moving surface," *Philosophical Transactions of the Royal Society of London. Series A, Mathematical and Physical Sciences*, vol. 249, no. 966, pp. 321–387, 1957.

[37] S. R. Brown and C. H. Scholz, "Closure of rock joints," *Journal of Geophysical Research: Solid Earth*, vol. 91, no. B5, pp. 4939–4948, 1986.